Am J Transl Res 2020;12(5):1491-1514
www.ajtr.org /ISSN:1943-8141/AJTR0109004

Review Article

PET imaging of macrophages in cardiovascular diseases

Xiang Li[1,2], Zachary T Rosenkrans[3], Jing Wang[1], Weibo Cai[2,3]

[1]Department of Nuclear Medicine, Xijing Hospital, Fourth Military Medical University, Xi'an 710032, Shaanxi, China; Departments of [2]Radiology and Medical Physics, [3]Pharmaceutical Sciences, University of Wisconsin-Madison, Madison, WI 53705, USA

Received February 10, 2020; Accepted March 14, 2020; Epub May 15, 2020; Published May 30, 2020

Abstract: Cardiovascular diseases (CVDs) have been the leading cause of death in United States. While tremendous progress has been made for treating CVDs over the year, the high prevalence and substantial medical costs requires the necessity for novel methods for the early diagnosis and treatment monitoring of CVDs. Macrophages are a promising target due to its crucial role in the progress of CVDs (atherosclerosis, myocardial infarction and inflammatory cardiomyopathies). Positron emission tomography (PET) is a noninvasive imaging technique with high sensitivity and provides quantitive functional information of the macrophages in CVDs. Although ^{18}F-FDG can be taken up by active macrophages, the PET imaging tracer is non-specific and susceptible to blood glucose levels. Thus, developing more specific PET tracers will help us understand the role of macrophages in CVDs. Moreover, macrophage-targeted PET imaging will further improve the diagnosis, treatment monitoring, and outcome prediction for patients with CVDs. In this review, we summarize various targets-based tracers for the PET imaging of macrophages in CVDs and highlight research gaps to advise future directions.

Keywords: Macrophages, positron emission tomography (PET), cardiovascular diseases (CVDs), atherosclerosis, myocardial infarction, cardiac sarcoidosis, myocarditis, pericarditis

Introduction

Cardiovascular diseases (CVDs) account for an immense health and economic burden in the United States and worldwide [1]. According to a report from the American Heart Association (AHA) in 2016, more than 121.5 million individuals are afflicted with CVDs. It is estimated that the annual direct and indirect costs of CVDs are $351.2 billion. CVDs are the leading cause of death in the United States [2].

Macrophages have been implicated in several CVDs, including the most prevalent CVDs with high morbidity and mortality such as atherosclerosis, myocardial infarction and inflammatory cardiomyopathies [3, 4]. In atherogenesis, macrophages are involved in the lesion initiation stage and advanced progression [5-7]. Apolipoprotein B-containing lipoproteins (apoB-LPs) accumulate at vascular intima and undergo a series of modifications, which triggers the recruitment of monocytes from the spleen and bone marrow. The infiltrated monocytes then differentiate into macrophages and take up the modified lipoprotein, thereby becoming "foam cells" [8, 9]. As the lesion expands, the lumen becomes narrow and may induce an ischemic event, such as angina pectoris [10]. During the subsequent progression, under endoplasmic reticulum stress, the macrophage derived foam cells undergo apoptosis and necrosis, which contributes to the formation of necrotic cores [11]. Enzymes secreted by macrophages, such as matrix metalloproteinases (MMPs), further erode the fibrous cap and makes plaque vulnerable to rupture and thrombosis [12]. Once the artery is completely occluded by in situ plaque, or thrombus derived from plaque rupture, the acute ischemic events (myocardial infarction or stroke) is triggered [13]. Following myocardial infarction, monocyte-derived macrophages infiltrate the infarcted heart within 24 hours. During the early phase (days 0-3), the infiltrating macrophages primarily secrete pro-inflammatory cytokines (TNF-α, IL-β, IL-6) and matrix proteases (MMPs) to clear dying cell debris. After approximately 5-7 days, these macro-

phages switch from a pro-inflammatory state to a pro-reparative state, secreting TGFβ1 and IL-10 to promote healing and decrease inflammation [14-16]. Macrophages have also been implicated in other inflammatory cardiovascular disease, such as cardiac sarcoidosis [17], myocarditis [18], peri/endocarditis [19] and vasculitis [20]. As such, macrophage tracking is important to aid early diagnosis, monitoring of disease activity and progression, treatment evaluation, and outcome prediction in CVDs.

Traditional imaging techniques such as computed tomography (CT) or magnetic resonance (MR) provide anatomical information but supply limited functional information. Positron emission tomography (PET) is an important nuclear imaging technique that can fill in this void [21]. Compared with other functional imaging modalities, such as optical fluorescence or bioluminescence, PET provides limitless penetration, quantitative accuracy, high sensitivity at picomolar level, and is easily translated to the clinic [21-23]. However, PET is limited in its morphological delineation ability due to low spatial resolution. Thus, hybrid PET/CT or PET/MR imaging has been increasingly applied preclinically and clinically to acquire both functional and anatomical information [24]. With the support of a cyclotron, short half-life isotope (^{11}C, ^{18}F, ^{68}Ga) and long half-life isotope (^{89}Zr, ^{64}Cu) can meet nearly any labelling requirement of small molecules, large antibodies, or nanoparticles [25-27]. Therefore, PET imaging incorporated applications hold excellent potential for non-invasively tracking macrophages in CVDs.

Currently, the glucose metabolism-based tracer, ^{18}F-FDG, is the most commonly-investigated PET tracer for imaging macrophages in CVDs. To date, previous reviews have excellently summarized relevant studies on FDG-based macrophages imaging in CVDs [28-31]; While ^{18}F-FDG is readily available and has been widely employed in both the preclinical and clinical setting, some limitations still exist. First, it is a non-specific probe that can accumulate in other metabolically active cells and introduces background signal [32]. Moreover, ^{18}F-FDG is affected by blood glucose levels, insulin levels and drug interference, which limits application in diabetic patients with hyperglycemia [33]; Additionally, FDG imaging of the macrophages in heart requires advanced patient preparation (fasting overnight or high fat diet) to suppress physiological signal from myocardial uptake. However, these methods are not always successful and feasible, particularly to MI patients or those in a poor physical condition. Standard methods to make a repeatable and effective suppression are still lacking, increasingly the likelihood of inaccurate quantification [30, 33, 34]. Thus, the development of specific and convenient PET tracers is still required.

Herein, we systematically review the currently available PET tracers other than ^{18}F-FDG for the imaging of macrophages and summarize their applications in CVDs. These tracers can be generally classified into metabolism or proliferation based, chemokine receptor-targeted, somatostatin receptor-targeted, translocator protein targeted, mannose receptor-targeted, secreted enzymes-targeted, nanoparticle-based, antibody-based, and other potential targets. Some potential tracers currently applied in other diseases will also be discussed. We also discuss the current research limitations and highlight future directions. We believe the macrophage targeted PET imaging will deepen our understanding of macrophages' function in CVDs, as well as facilitate early diagnosis, risk stratify and treatment monitoring, and provide benefits to CVDs patients in the future.

Metabolism & proliferation based PET imaging

Amino acid metabolism: ^{11}C-methionine

L-[methyl-^{11}C] methionine (^{11}C-methionine, ^{11}C-MET) is a radioisotope-labeled amino acid that is take up by more metabolically active cells and has been used in PET oncology applications [35]. Morooka M and colleagues first investigated the uptake of ^{11}C-methionine in myocardial infarction/reperfusion patients. They found the highest accumulation of ^{11}C-methionine in the infarcted area, whereas ^{201}Tl and ^{18}F-FDG uptake decreased (**Figure 1A**) [36]. A similar phenomenon was also reported in a rat infarction/reperfusion model using ^{14}C-methionine. The tracer uptake closely corresponded to macrophage infiltration based on histology at day 3-7 [37]. Cellular uptake assay indicated the uptake of isotope-labeled methionine in pro-inflammatory M1 macrophages was higher than other cells and that the PET signal could be modulated with anti-integrin treatment [38].

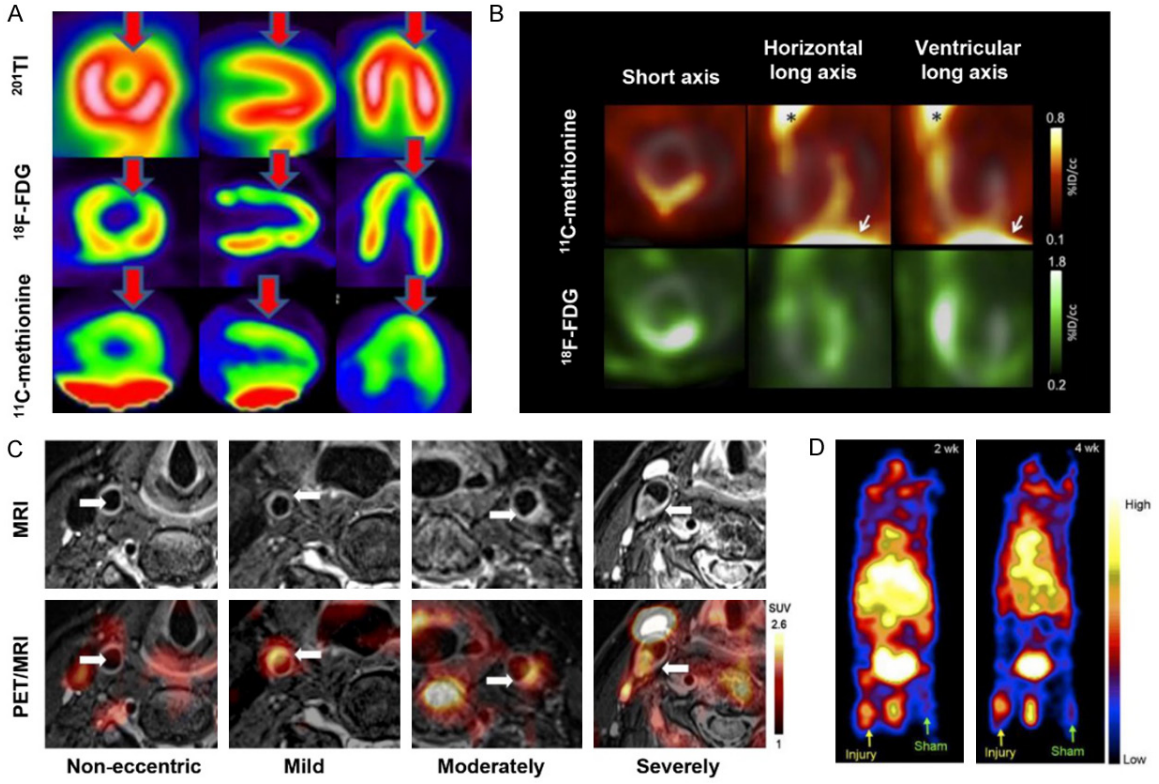

Figure 1. A. ^{11}C-methionine PET, ^{18}F-FDG PET and ^{201}Tl SPECT imaging in an 43-years-old acute myocardial infarction patient. Infarction zone (red arrow) in anterior wall exhibited decreased uptake on ^{201}Tl and ^{18}F-FDG images, but relatively increased uptake on ^{11}C-methionine images; B. ^{11}C-methionine and ^{18}F-FDG PET imaging in an experimental autoimmune myocarditis (EAM) rat, colocalization of focal myocardial uptake of both tracers is shown. ^{11}C-methionine uptake was also observed in extracardiac areas (asterisk) and liver (arrowheads); C. ^{68}Ga-Pentixafor PET/MRI imaging of atherosclerotic carotid plaques. The lesions were semi-quantitatively classified into four groups based on the cross-sectional luminal obstructive features on T2-weighted MRI, including Non-eccentric (non-significant luminal obstruction), Mild (≤10%), moderately (>10%), severely (≥25%) the white arrow indicate the arterial regions of interest; D. CCR5 targeted ^{64}Cu-DOTA-vMIP-II PET imaging in a atherosclerotic mice model at 2 and 4 weeks. ^{64}Cu-DOTA-vMIP-II significantly accumulated at the site of injury lesions, whereas the sham site had only weak accumulation. Adapted with permission from [36, 39, 63, 70].

Maya et al. compared the distribution of ^{11}C-methionine and ^{18}F-FDG in a rat autoimmune myocarditis model, which revealed by histology that both tracers colocalized at inflammatory lesions. An excellent positive correlation also existed between ^{11}C-methionine and ^{18}F-FDG. However, the contrast of ^{11}C-methionine was lower than ^{18}F-FDG for discriminating inflammatory and noninflammatory lesions (**Figure 1B**) [39] (**Table 1**).

Choline metabolism: ^{11}C-choline and ^{18}F-FCH

Cholines are involved in the metabolism of cell membrane lipids and is regulated by choline kinase, which is upregulated in tumor cells and activated macrophages [40]. In contrast to ^{18}F-FGD, radiolabeled choline or fluorocholine is not significantly taken up by myocardium. Currently, ^{11}C-choline and ^{18}F-FCH have garnered the most attention in imaging of macrophages of CVDs. Kato et al. retrospectively analyzed the uptake of ^{11}C-choline in plaques from 93 elderly prostate cancer patients. They found that 95% of patients have positive PET results and that the tracer uptake rarely colocalized with calcification [41]. This finding was subsequently supported by mouse model study, which found a 2.6-fold higher uptake in inflamed plaque than the healthy vessel wall using ex vivo autoradiography [42].

Compared to the short half-life of ^{11}C, ^{18}F-fluorocholine (^{18}F-FCH) is more suitable in the clinical setting for choline-based imaging. Matter et al. found ^{18}F-FCH uptake at murine

Table 1. Summary of metabolism/proliferation based, chemokine receptor-targeted, SSTR-targeted probes illustrated in the present review

Target	Disease	Preclinical/clinical	Radiotracer
Amino acid metabolism	Myocardial infarction	Clinical	^{11}C-methionine [36, 38]
		Preclinical	^{14}C-methionine [37] ^{11}C-methionine [38]
	Myocarditis	Preclinical	^{11}C-methionine [39]
Choline metabolism	Atherosclerosis	Preclinical	^{11}C-Choline [42]; ^{18}F-FCH [43]
		Clinical	^{11}C-Choline [41]; ^{18}F-FCH [44, 45]
Proliferation	Atherosclerosis	Preclinical/clinical	^{18}F-FLT [47]
	Abdominal aortic aneurysms	Preclinical	^{18}F-FLT [48]
Chemokine receptors			
CXCR4	Myocardial infarction	Preclinical	^{68}Ga-pentixafor [57]
		Clinical	^{68}Ga-pentixafor [57-59, 158]
	Atherosclerosis	Preclinical	^{68}Ga-pentixafor [60]
		Clinical	^{68}Ga-pentixafor [60-65]
CCR2	Cardiac injury/Myocardial infarction	Preclinical	^{68}Ga-DOTA-ECL1i [69]
CCR5	Atherosclerosis	Preclinical	^{64}Cu-DOTA-vMIP-II [70]
	Vascular injury/Atherosclerosis	Preclinical	^{64}Cu-DOTA-DAPTA-comb [71]; ^{64}Cu-DOTA-Vmip-II-comb [72]
Somatostatin receptors (SSTR)	Myocardial infarction	Preclinical	^{68}Ga-DOTA-TATE and ^{68}Ga-citrate [90]
		Clinical	^{68}Ga-DOTA-TOC [86]
	Sarcoidosis/Myocarditis/Pericarditis	Clinical	^{68}Ga-DOTA-TOC [84-87]; ^{68}Ga-DOTA-NOC [88]
			^{68}Ga-DOTA-TATE [89]
	Atherosclerosis	Preclinical	^{68}Ga-DOTA-TATE [75]; ^{68}Ga-DOTA-NOC [79]; ^{18}F-FDR-NOC [79]
		Clinical	^{68}Ga-DOTA-TATE [76-78, 82, 83]; ^{64}Cu-DOTA-TATE [80, 81]
			^{68}Ga-DOTA-TOC [80]

plaque correlated well with Oil staining and macrophages staining with better sensitivity compared to ^{18}F-FDG [43]. A small retrospective study including five patients showed that 17 negative lesions were verified among the 31 detected vessel wall alterations. 16 of the 17 lesions were further identified as solely calcified lesions, indicating relatively stable plaque uptake of ^{18}F-FCH [44]. Voo S and co-workers performed a prospective clinical study on the feasibility of ^{18}F-FCH to identify vulnerable plaques. Ten stroke patients with over 70% carotid artery stenosis were involved in their study. ^{18}F-FCH uptake in ipsilateral symptomatic carotid plaques significantly correlated with CD68^{+} macrophage staining in carotid endarterectomy specimens. Importantly, compared to the contralateral asymptomatic carotid arteries, ipsilateral symptomatic plaques exhibited higher uptake, indicating ^{18}F-FCH is promising for identifying vulnerable plaques [45] (**Table 1**).

Proliferation: ^{18}F-FLT

3'-deoxy-3'-[^{18}F]fluorothymidine (^{18}F-FLT) is a classic PET tracer traditionally used for visualizing tumor proliferation [46]. In 2015, Ye et al. investigated the possibility of ^{18}F-FLT PET imaging for monitoring macrophages proliferation in atherosclerotic mice, a rabbit model, and patients. The PET results revealed an increased ^{18}F-FLT signal in atherosclerotic lesions in animal models and patients. In vivo results were further verified by autoradiography and flow cytometry. Apart from plaques, significant ^{18}F-FLT uptake was also observed in spleen and bone marrow, which may due to the proliferation of hematopoietic stem and progenitor cells. Interestingly, they further found the signal correlated with the duration of a high cholesterol diet, and the signal was reduced by fluorouracil, a proliferation inhibitor [47]. Since macrophage proliferation is closely related to the progression of plaque, ^{18}F-FLT PET imaging may serve as a tool for monitoring plaque progression and therapy. Recently, Gandhi R and colleagues also investigated the feasibility of ^{18}F-FLT PET imaging in abdominal aortic aneurysm, By using an AngII-induced mice model, they confirmed the uptake of ^{18}F-FLT in 14-day aortae was greater than that in 28-day and control, and the uptake also correlated positively with aortic volume [48] (**Table 1**).

Chemokine receptors

Chemokines exert chemotactic effects on cells via binding with its receptor. Chemokine family can be divided into the major (CC, CXC) and the minor (C and CX3C) groups based on the N-terminal cysteine residues [49, 50]. Among the various chemokine receptors, CXCR4, CCR2, and CCR5 garnered prominent attention in recent years due to their high expression on monocytes/macrophages and closely related leukocytes as well as their crucial roles in CVDs progression [51-54].

CXCR4

CXCR4-CXCL12 is involved in leukocyte recruitment to the injured region in CVDs. The inhibition of CXCR4-CXCL12 (SDF-1) has shown benefits for acute myocardial infarction and atherosclerosis [52]. Driven by CXCR4 targeted PET imaging in tumor [55, 56], Thackeray and colleagues evaluated ^{68}Ga-pentixafor PET imaging in myocardial infarction disease. In a murine model, significantly increased signal was observed in the infarct region, which could also be blocked by a CXCR4 antagonist and attenuated by long-term enalapril treatment. The autoradiography results colocalized with the presence of macrophages and granulocytes in histology, indicating this PET signal originates from recruited inflammatory cells. Interestingly, the authors found variable degree of ^{68}Ga-pentixafor uptake in MI patients and the signal correlated with the bone marrow uptake [57]. At the same time, Lapa et al. reported the uptake of ^{68}Ga-pentixafor in 3 of 7 AMI patients (5-10 days after MI) [58]. They further verified 17/22 positive imaging in another study (patients on 2-13 days after MI), in which the ^{68}Ga-pentixafor PET signal not only negatively correlated with the time point of imaging, but also has a correlation with scar volumes assessed by CMR. In addition, the tracer signal could be observed up to 13 days after MI [59].

In 2017, ^{68}Ga-pentixafor was first evaluated in atherosclerotic plaques in a rabbit model and eight patients. The authors demonstrated high tracer uptakes in plaques of rabbit model by PET/MR. The signal was reduced by 40% with pre-injection of CXCR4 inhibitor. Ex vivo analysis showed ^{125}I-pentixafor uptake on autoradiography colocalized with the macrophage-rich region in plaque and correlated with the expres-

sion of CXCR4. Importantly, they further identified intense tracer uptake in two carotid atherosclerotic patients with over 50% carotid stenosis. The additional immunohistochemistry staining of human plaques showed that CXCR4 mostly located in the macrophages-rich area but not in lymphocytes or endothelial-rich areas [60]. The next year, two groups respectively investigated the relationship of ^{68}Ga-pentixafor uptake and cardiovascular risks with a larger cohort of patients. Weiberg et al. retrospectively analyzed 51 patients who underwent ^{68}Ga-pentixafor PET/CT imaging. They found that the tracer uptake was associated with cardiovascular risk factors and increased with the number of risk factors (age, arterial hypertension, hypercholesterolemia, history of smoking, prior cardiovascular events) [61]. Li and colleagues performed ^{68}Ga-pentixafor PET/MR imaging in 38 patients, which revealed those with high uptake of tracer (mean TBR_{max}>1.7) exhibited a higher incidence of hypertension, hypercholesterolemia, diabetes, and history of cardiovascular disease. These results illustrate the potential of ^{68}Ga-pentixafor in the characterization of atherosclerosis [62]. By taking advantage of MR in delineation of plaques, the same group involved 72 additional patients and divided them into four groups (non-eccentric, mild, moderately and severely) according to the degree of carotid plaque. They found the ^{68}Ga-pentixafor uptake was absent in the non-eccentric group but significantly increased among the other three groups. However, no statistical differences exist between the other three groups. Additionally, they correlated the MRI results with histological evidence and found high expression of CXCR4 within inflamed atheroma and pre-atheroma, but not the fibro-atheroma with low macrophages. This indicated that ^{68}Ga-pentixafor PET imaging can recognize plaques with inflammatory activity (**Figure 1C**) [63]. They further proved ^{68}Ga-pentixafor PET imaging could identify more lesions than ^{18}F-FDG PET, with a weak correlation between the two probes [64]. Using the motion-corrected technique, Derlin et al. showed ^{68}Ga-pentixafor PET/CT imaging could identify small coronary atherosclerotic plaques in patients after acute myocardial infarction [65] (**Table 1**).

CCR2

In 2016, a seven amino acid peptide (LGTFLKC) with excellent inhibition property to CCR2 was identified and named extracellular loop 1 inverso (ECL1i) by the authors [66]. Subsequently, it was developed into a PET imaging tracer by Liu et al. for in vivo imaging of $CCR2^+$ cells in an ischemia-reperfusion injury model after lung transplantation [67] and a LPS-induced lung inflammation model [68]. In 2019, CCR2 targeted PET imaging was first investigated in cardiac injury by Heo and colleagues. The investigators used ^{68}Ga to radiolabel the ECL1i peptide (^{68}Ga-DOTA-ECL1i), which showed high tracer uptake at cardiac injury lesions in a cardiomyocyte ablation model as well as in a myocardial infarction/reperfusion (I/R) model. However, in a CCR knock-out mice model, minimal signal was detected. To further support the specificity, they performed autoradiography with MI patients' heart tissue (acute and chronic). The human specimens exhibited heterogeneous radioactive signal levels, which could also be blocked. the signal was correlated with the number of $CD68^+$ macrophages and with $CD68^+/CCR2^+$ cells, but not with $CD68^+/CCR2^-$ cells, implying the tracer could specifically recognize $CCR2^+$ macrophages and monocytes [69] (**Table 1**).

CCR5

In 2013, Liu and colleagues radiolabeled a viral macrophage inflammatory protein II (vMIP-II) with ^{64}Cu (^{64}Cu-DOTA-vMIP-II) and used PET imaging to monitor the distribution in a vascular injury-accelerated atherosclerosis model. They found 3-fold accumulation at the injury site in the model compared to the sham site (**Figure 1D**). Compared with ^{18}F-FDG, the tracer displayed better accumulation at injury sites. The PET signal could also be blocked by eight chemokines. Among them, CCR5 and CXCR4 antagonists exhibited the most pronounced blocking effects [70]. Subsequently, to improve tracer accumulation, the authors designed two CCR5 targeted nanoparticle probes, ^{64}Cu-DOTA-Vmip-II-comb and ^{64}Cu-DOTA-DAPTA-comb. These nano-based tracers displayed higher uptake and contrast ratios when compared to previous tracers without nanoparticle conjugation [71, 72] (**Table 1**).

Somatostatin receptor (SSTR)

Somatostatin (SST) is a cyclic polypeptide with broad inhibitory effects on the release of other secretory proteins. SST receptors (SSTRs) are

G-protein-coupled receptors with five subtypes, which are expressed on immune cells and neuroendocrine tumors [73]. Thus, PET imaging probes targeting SSTRs have been previously developed and used for diagnosing neuroendocrine tumor [74]. Since 2010, SSTR-targeted tracers have been employed for cardiovascular imaging.

^{68}Ga-DOTA-TATE is a radiotracer selectively binding to the SSTR2. The accumulation of ^{68}Ga-DOTA-TATE at atherosclerotic plaques was reported in a mouse model. The autoradiography result displayed the tracer uptake co-localized with the macrophage-rich plaques from histology, indicating ^{68}Ga-DOTA-TATE is suitable for imaging of macrophages in plaques [75]. Three retrospective clinical studies demonstrated the detectability of ^{68}Ga-DOTA-TATE in human plaques in coronary or large arteries. All of the studies found that individuals with prior cardiovascular events exhibited higher tracer uptake in plaque [76-78]. Rinne et al. compared the three SSTR-targeted tracers ^{68}Ga-DOTA-TATE, ^{68}Ga-DOTA-NOC and ^{18}F-FDR-NOC in atherosclerotic mice model. They found that ^{68}Ga-DOTA-TATE and ^{68}Ga-DOTA-NOC were superior for imaging plaque than ^{18}F-FDR-NOC [79]. In addition, another group investigated a long half-life isotope radiolabeled tracer ^{64}Cu-DOTA-TATE. They found that, compared with ^{68}Ga-DOTA-TOC, ^{64}Cu-DOTA-TATE had enhanced accumulation within plaque in large arteries. The ^{64}Cu-DOTA-TATE uptake was associated with cardiovascular risk factors [80] and CD163 gene expression, which has been reported to be highly expressed on activated M2 macrophages [81]. In 2017, a prospective clinical study named “VISION” involved 42 atherosclerotic patients systematically investigated ^{68}Ga-DOTA-TATE for detecting inflamed plaque. In this study, the authors demonstrated ^{68}Ga-DOTA-TATE could specifically bind with the SST2 receptor, which also colocalized with CD68^{+} macrophages. ^{68}Ga-DOTA-TATE was better able to discriminate high-risk and low-risk coronary lesion compared to ^{18}F-FDG [82]. However, another prospective study involving 20 patients, questioned the ability of ^{68}Ga-DOTA-TATE PET imaging to discriminate the symptomatic and asymptomatic carotid plaques, citing the lack of SST2 expression on excised human plaques [83].

SSTR2-targeted PET imaging in a cardiac sarcoidosis patient was first reported by Reiter et al. (**Figure 2A**) [84]. The same group further carried out two clinical studies to investigate SSTR targeted PET/CT imaging for detecting myocardial inflammation compared to cardiac magnetic resonance (CMR). Patients with cardiac sarcoidosis (CS) [85] or peri-/myocarditis, sub-acute myocardial infarction (MI) [86] were involved. Based on segment analysis, PET and CMR displayed high concordant results (CS: 96.1%; Peri-/myocarditis or MI: 85.3%), except a small portion of patients or segments different between the two modalities. Although it is hard to make a clear conclusion due to the lack of enough histopathologic data, it indicated that the combination of the two modalities (PET/MR) might be an optimal diagnostic approach. Another similar pilot study involving 17 histologically proven CS-positive patients revealed that only one patient displayed positive PET/CT results compared to the five positive patients verified by CMR. This discrepancy was attributed to treatment at the time of PET imaging, implying ^{68}Ga-DOTA-TOC PET/CT is helpful to monitor disease activity. This technique would also be particularly advantageous for individuals with contraindications to CMR, such as patients with pacemaker [87]. However, given the small cohort of patients, the value of ^{68}Ga-DOTA-TOC PET imaging requires further evaluation. Gormsen and co-workers performed a comparative study of ^{68}Ga-DOTA-NOC and ^{18}F-FDG in 19 suspected CS patients. They found that ^{68}Ga-DOTA-NOC PET imaging displayed higher diagnostic accuracy and better interobserver agreement than FDG-PET. The inferiority of FDG imaging may be ascribed to the incomplete suppression of physiological myocardial uptake by fasting [88]. In contrast, another recent study suggested decreased sensitivity of ^{68}Ga-DOTA-TATE in detecting CS inflammation compared with FDG. The authors also found weak SSTR2 expression in all three sarcoid heart specimens examined by immunostaining [89]. MI mice study indicated that neither ^{68}Ga-citrate or ^{68}Ga-DOTA-TATE is superior to FDG PET imaging for detecting post-MI inflammation [90]. Heterogeneous results have raised more questions on the diagnostic ability of SSTR2-targeted PET imaging of macrophages in inflammatory cardiomyopathies that must be reconciled in future studies (**Table 2**).

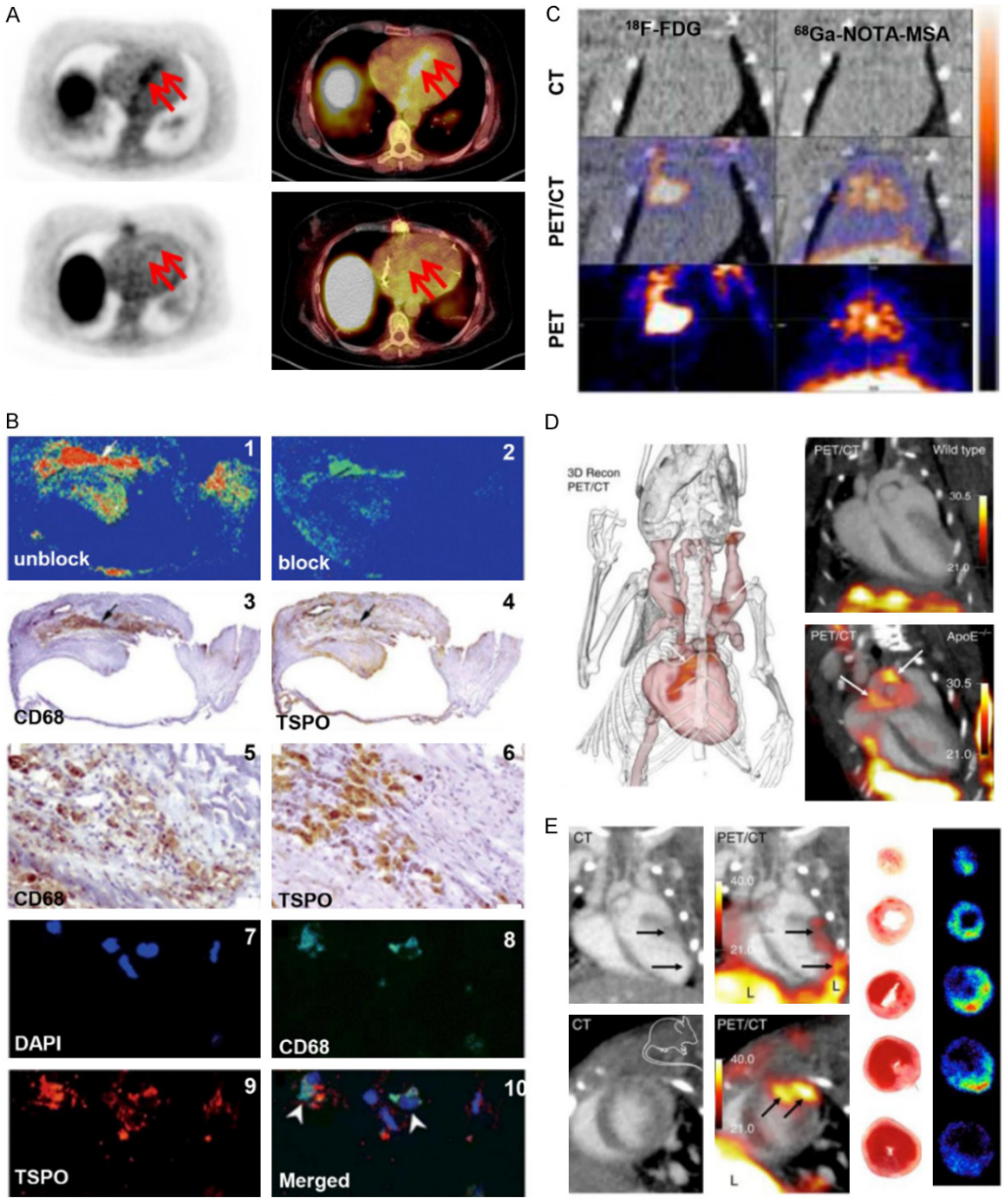

Figure 2. A. SSTR-targeted ^{68}Ga-DOTA-TOC PET/CT imaging in a 54-year-old patient with cardiac sarcoidosis. The red arrow in upper images indicate the inflammatory area. The lower images are ^{68}Ga-DOTA-TOC PET/CT imaging after 10-months systemic treatment. B. The verifying for the specificity of TSPO-targeted tracer PK11195, in atherosclerotic samples from patients who underwent carotid endarterectomy. Representative autoradiography, immunohistochemistry and immunofluorescence microscopy. The autoradiography showed that ^{3}H-PK11195 binding with plaques and unlabeled PK11195 could block its binding (1-2). The immunohistochemistry showed the positive area of macrophage marker CD68 (3 and 5) and TSPO (4 and 6) respectively. 7-10 were immunofluorescence staining of DAPI, CD68. TSPO and merged image respectively. C. MR-targeted ^{68}Ga-NOTA-MSA PET imaging of macrophages compared with ^{18}F-FDG PET imaging in myocarditis model. D. ^{18}F-Macroflor PET/CT imaging of macrophages in aortic plaques of mice with atherosclerosis. Representative images of PET/CT in wild type mice (upper) and atherosclerotic mice model (lower); Three-dimensional image of PET/CT in atherosclerotic mice model. PET signal was in red (arrows); E. ^{18}F-Macroflor PET/CT imaging of macrophages in murine myocardial infarction model. Long axis view (upper row) and short axis view (lower row); Ex vivo autoradiography and it corresponding TTC staining of infarct heart at day 2 post-MI. Adapted with permission from [84, 96, 108, 139].

Table 2. Summary of TSPO, MR, MMP, MPO targeted or nanoparticle-based probes illustrated in the present review

Target	Disease	Preclinical/clinical	Radiotracer
Translocator protein (TSPO)	Atherosclerosis/vascular injury	Preclinical	^{11}C-PK11195 [94]; ^{18}F-FEDAA1106 [97]; ^{18}F-PBR06 [98]
			^{18}F-FEMPA [99]; ^{18}F-GE-180 [100]
		Clinical	^{11}C-PK11195 [96]
	Abdominal aortic aneurysms	Clinical	^{11}C-PK11195 [95]
	Myocardial infarction	Preclinical/clinical	^{18}F-GE-180 [101]
	Myocarditis	Preclinical	^{18}F-PBR28 [102]; ^{18}F-CB251 [102]
Mannose receptor (MR)	Atherosclerosis	Preclinical	^{18}F-FDM [104]; ^{68}Ga-NOTA-MSA [105]; ^{68}Ga-MMR [106]
			^{68}Ga-anti-MMR Nb [107]
	Myocarditis	Preclinical	^{68}Ga-NOTA-MSA [108]
Secreted enzymes			
MMPs	Myocardial infarction	Preclinical	^{68}Ga-DOTA-MMP-2/9 targeted peptide [114]
	Atherosclerosis	Preclinical	^{68}Ga-DOTA-TCTP-1 [116]
MPO	Myocardial infarction	Preclinical	^{18}F-MAPP [117]; ^{11}C-AZD3241 [124]
Nanoparticles (NPs)			
Modified dextran	Atherosclerosis	Preclinical	^{64}Cu-TNP [132]; ^{89}Zr-DNP [133]
High density lipoprotein	Atherosclerosis	Preclinical	^{89}Zr-AI-HDL and ^{89}Zr-PL-HDL [134]
Hyaluronan	Atherosclerosis	Preclinical	^{89}Zr-HA-NP [135]
Dendrimers	Atherosclerosis	Preclinical	^{64}Cu-(LyP-1)4-dendrimer [136]
Porphysome	Myocardial infarction	Preclinical	^{64}Cu-folate-porphysome [137]
Mesoporous silica	Atherosclerosis	Preclinical	^{18}F-DBCO-MSNs [138]
Polyglucose	Atherosclerosis/MI	Preclinical	^{18}F-Macroflor [139]

Translocator protein (TSPO)

The 18 kDa-protein translocator protein (TSPO), previously known as peripheral benzodiazepine receptor (PBR), is localized on the outer mitochondrial membrane. TSPO is involved in several essential cellular functions, such as cholesterol transport or steroidogenesis [91, 92]. TSPO is expressed in both M1 and M2 macrophages, and some studies reported a higher expression in M2 macrophages [93].

The first generation TSPO-targeted PET tracer, ^{11}C-PK11195 has shown higher accumulation at inflamed plaques compared to non-inflamed plaques in atherosclerotic mice model, but a comparable uptake in healthy artery walls may limit in vivo imaging applications [94]. Another study did not observed any aortic uptake in asymptomatic abdominal aortic aneurysms patients either [95]. However, a subsequent clinical study demonstrated the feasibility of ^{11}C-PK11195 PET for imaging of intraplaque macrophages. Histologic staining on patient carotid plaque verified the tracer specificity since TSPO and CD68 co-localized with tracer uptake on autoradiography (**Figure 2B**). Moreover, they suggested the higher ^{11}C-PK11195 target-to background ratio (TBR) combined with lower CT attenuation could distinguish recently symptomatic and asymptomatic plaques in patients [96].

The nonspecific binding and short half-life of ^{11}C prompted the design of new generation tracers. To date, ^{18}F-FEDAA1106, ^{18}F-PBR06, ^{18}F-FEMPA and ^{18}F-GE-180 have been investigated in inflammatory vascular models. ^{18}F-FEDAA1106 showed significant uptake in vascular injury regions and displayed higher specificity to discriminate inflamed and non-inflamed vasculature compared to ^{18}F-FDG [97]. ^{18}F-PBR06 PET imaging revealed a higher uptake in atherosclerotic plaques of 32 weeks than that of 22 weeks, implying the potential for evaluating plaque progression [98]. Hellberg et al. reported that both ^{18}F-FEDAA1106 [99] and ^{18}F-GE-180 [100] accumulated in atherosclerotic plaques and the signal correlated well with the distribution of macrophages. However, comparable uptake in healthy vessel walls, attributed to the ubiquitous nature of TPSO expression, limits in vivo PET imaging applications. Clinical translation may be possible since interspecies differences exist.

The third generation TSPO-targeted tracer ^{18}F-GE-180 was investigated in myocardial infarction. In MI mice model, elevated ^{18}F-GE-180 signal could be observed at 1 weeks after infarction and was localized to CD68^{+} macrophages. After interval decline at 4 weeks, the signal then increased in remote myocardium where less inflammatory cells exist at 8 weeks, implying the complexity of TSPO signal which could also reflect mitochondrial impairment. Interestingly, obvious ^{11}C-PK11195 PET signal was further verified on both heart and brain in a patient after MI, suggesting the immune activation may exist at the heart-brain axis [101]. Another two TSPO tracers have been investigated in rat myocarditis model. In this study, ^{18}F-PBR28 displayed no significant elevation in the model, but ^{18}F-CB251 did [102] (**Table 2**).

Mannose receptor (CD206)

A highly effective endocytic receptor, the mannose receptor (MR) expression has been reported on macrophages, dendritic cells and nonvascular endothelium [103]. Consensus is that MR is generally expressed on M2 macrophages. Staining of atherosclerotic coronary sections from patients that have suffered sudden cardiac death revealed intense MR positive M2 macrophages in the unstable plaques, which featured with thin-cap fibroatheromas, but almost no MR expression in stable plaques [104].

Mannose is a C2-epimeric sugar molecule with a chemical structure similar to glucose; the only difference is the opposite orientation of oxygen and hydroxyl groups on the second carbon atom. Mannose binds on macrophages via MRs and enters cells via glucose transporters (GLUTs) [104]. Tahara et al. found the uptake of ^{18}F-labeled mannose (^{18}F-FDM) in rabbit plaque is comparable to ^{18}F-FDG and was proportional to macrophage density in tissue. More importantly, using six sets of cell experiments, the authors demonstrated the specific binding of FDM to MR and a macrophage uptake increase of more than 35% for ^{18}F-FDM compared to ^{18}F-FDG [104]. Mannosylated human serum albumin (MSA), a 6-8 nm protein, binds with macrophages via terminal mannose residues. It was previously developed for imaging of sentinel lymph nodes, but Kim and colleagues recently used ^{68}Ga radiolabeled NOTA-MSA for plaque imaging in a rabbit model. The ^{68}Ga-NOTA-MSA

uptake in plaque was significantly higher than in healthy arteries and was comparable to ^{18}F-FDG. Cell uptake and blocking experiments verified the binding specificity to M2 macrophages [105].

Senders et al. evaluated a MR targeted nanobody, which was previously used in tumor PET imaging, in atherosclerotic murine and rabbit models after radiolabeling with ^{64}Cu or ^{68}Ga. In the mice model, the ^{64}Cu-MMR showed significant accumulation in the aortic root and arch. Autoradiography and histologic staining for macrophages proved the tracer specificity. Subsequent ^{64}Cu-MMR PET/MR imaging in a rabbit model indicated tracer uptake positively correlated with vessel wall area, but not with the FDG uptake. To meet clinical demands, short-lived ^{68}Ga was also used for radiolabeling. Compared with 4-month results, the tracer uptake, vessel wall area and vascular permeability progressively increased at 8 months in rabbit models. ^{68}Ga-MMR autoradiography also positively correlated with CD206 expression, indicating ^{68}Ga-MMR PET/MR has potential to reflect disease progression and the amount of CD206$^+$ macrophages [106]. Another MR targeted nanobody (^{68}Ga-anti-MMR Nb) has also been studied in ApoE (-/-) atherosclerotic mice model. The positive PET results matched with autoradiographs and Sudan-IV-staining. Immunofluorescence staining revealed MR was predominantly expressed in macrophages located in the fibrous cap layer and shoulder region of the plaques [107].

MR-targeted PET imaging was also investigated in myocarditis disease. The infiltration of MR-positive macrophages was confirmed in a rat myocarditis model and using human histological samples (**Figure 2C**). The left ventricle uptake of ^{68}Ga-NOTA-MSA in myocarditis was 1.8-fold higher compared with the control group, which could be reduced by cyclosporine-A treatment. Cell and tissue block experiments demonstrated the specificity of ^{68}Ga-NOTA-MSA. Compared with echocardiography, the ^{68}Ga-NOTA-MSA PET imaging displayed early diagnosis efficiency for detecting myocarditis [108] (**Table 2**).

Macrophages enzymes

Metalloproteinases (MMPs)

Macrophages releases proteolytic matrix metalloproteinases (MMPs) that degrade the cardiac extracellular matrix or erode fibrotic plaque caps and as a result are involved in the cardiac remodeling or plaque rupture process in CVDs. Among them, type 2 and 9 MMPs have been investigated the most [12, 109, 110]. Molecular imaging of macrophages using MMPs targeted probes have received considerable attention over the recent decade.

While molecular imaging probes have been developed, their application as PET imaging tracers has been relatively unexplored. In 2005, Su and colleagues reported a SPECT probe, ^{99m}Tc-RP805, which could specifically bind to the activated catalytic domain of MMPs and displayed a fivefold uptake increase in the infarcted area and a twofold increase in the remote region of MI mice heart [111]. Another study from this group revealed that regional uptake of ^{99m}Tc-RP805 was highly concordant with ex vivo MMP-2 activity and the SPECT signal predicted late left ventricular remodeling [112]. Another activatable cell-penetrating peptide probe (ACPP) was described for imaging MMP activity in MI. ^{177}Lu and ^{125}I were chelated to the ends of this peptide. Once MMPs cleaved the middle of ACPP, the ^{125}I-peptide would be washed out and the ^{177}Lu-peptide remained. The authors observed a ten-fold uptake in the infarct myocardium compared to the remote region. However, it still requires an in vivo imaging investigation [113]. To develop an MMP-targeted PET probe, Kiugel et al. selected a peptide using a phage display technique. The peptide displayed a robust performance for targeting MMP-2/9 in a tumor model. Then it was radiolabeled with ^{68}Ga for PET imaging in a myocardial infarction rat model. Ex vivo autoradiography showed higher accumulation in the infarcted area compared to the remote area. Moreover, the tracer uptake also correlated with CD68$^+$ macrophages 7 days after MI. However, high blood signal, tracer instability, and slow clearance limit in vivo PET imaging applications [114].

MMP-targeted SPECT imaging probes for atherosclerosis have been summarized in a previous review by Lenglet et al. [115]. Recently, Kiugel et al. published a PET study for imaging of MMP in atherosclerotic plaques. However, they also observed low blood clearance and tracer instability that would limit applications. In an atherosclerotic murine model, a 1.8-fold uptake of ^{68}Ga-DOTA-TCTP-1 in plaque was

detected ex vivo, but it was not discernable with in vivo PET imaging, which may be ascribed to a low target-to-background ratio [116] (**Table 2**).

Myeloperoxidase (MPO)

Myeloperoxidase (MPO) is an important enzyme associated with oxidative stress and is secreted by neutrophils and pro-inflammatory M1 macrophages but not the anti-inflammatory M2 macrophages [117]. MPO is involved in early plaque formation since it impairs cholesterol transport. By oxidizing low-density lipoproteins (LDL) MPO aids in foam cell formation [118]. It has also been reported that MPO contributes to cardiac remodeling and heart failure following myocardial infarction [119]. As such, MPO is an exciting target for imaging macrophages in CVDs.

To date, there are limited MPO-targeted PET probes, though several MRI and SPECT imaging studies have been conducted. Chen et al. designed an MPO-Gd (bis-5HT-DTPA-Gd) probe for MR imaging and subsequently demonstrated its feasibility for imaging MPO activity in myocardial infarction and atherosclerotic plaque models [120-122]. Wu et al. radiolabeled bis-5HT-DTPA with ^{111}In for SPECT imaging in an atherosclerotic mice model. The probe showed high uptake in the aortic wall of atherosclerotic mice model, but the tracer elimination was significantly slower compared to WT mice. This may result from the increase in size after self-oligomerization of the probe induced by MPO oxidization [123].

The lower sensitivity and potential toxicity limit the application of these MR or SPECT tracers in a clinical setting. In 2015, the MPO inhibitor-based PET tracer ^{11}C-AZD3241 was found to enter the monkey brain [124]. However, the clinical application of the probe was still limited since the tracer only visualized the presence of MPO but not the activity and the short half-life of ^{11}C. To overcome these limitations, Wang et al. synthesized a ^{18}F-labeled PET tracer, ^{18}F-MAPP, which displayed high specificity and sensitivity, nontoxic, proper half-life, and crossed the blood-brain barrier. Similar to the mechanism of MPO-Gd, MPO could oxidize ^{18}F-MAPP and causes free radicals to bind to proteins and local retention of the radiotracer; thus the probe reflected MPO activity. The authors also demonstrated the feasibility and specificity of ^{18}F-MAPP in a mice myocardial infarction model and found the signal-background ratio was twice as high as MPO-Gd or its SPECT analogs, results promising for clinical application [117] (**Table 2**).

Nanoparticles (NPs) based PET imaging

Recently, PET imaging with NPs has garnered significant interest in CVDs [125]. As a multifunctional platform, nanoparticles could amplify the PET signal as well as carry therapeutic drugs, thus exhibit additional theranostic merits [126-128].

NPs based PET imaging of macrophages generally exploits the high endocytosis or micropinocytosis activity of macrophages [129, 130]. However, whether NPs can be taken up by macrophages at an injury site is complicated and is related to multiple factors including size, shape, surface properties, and opsonization. The general consensus is that NPs diameter between 10 and 300 nm are preferable for macrophages uptake at diseased sites. If much larger (over 1000 nm) or smaller (under 8 nm), NPs tend to accumulate in the liver and lungs or are cleared by the kidneys, respectively [131]. The choice of isotope for PET imaging depends on the circulation time of the NPs. Long-circulating nanomaterials require isotopes with long half-lifes, such as ^{89}Zr or ^{64}Cu. The clinical feasibility of short half-life isotopes such as ^{18}F or ^{68}Ga are more suitable to NPs that are rapily cleared [131].

In 2008, Nahrendorf et al. synthesized a ^{64}Cu-labeled trimodal (PET/MRI/optical) NP. The ^{64}Cu-TNP had a monocrystalline iron oxide NP MION as the core and was modified with a surface dextran coating. In ApoE-deficient mice models, ^{64}Cu-TNP displayed significant accumulation in the aortic root and arch, which correlated with MR and optical imaging results. Ex vivo autoradiography and Oil Red O staining corroborated that the sites where ^{64}Cu-TNP accumulated were macrophage-rich plaques. Flow cytometry of cellular suspensions from atherosclerotic plaque revealed macrophages contribute to 73.9% of overall signal. Compared with ^{18}F-FDG, ^{64}Cu-TNP PET signal was slightly higher and persisted longer [132]. Based on this work, this group further developed a core-free dextran nanoparticles (DNP) using clinical-

ly approved components and modified them with a ^{89}Zr chelator and a near-infrared fluorochrome (VT680) for PET/NIR imaging of atherosclerotic plaque. High uptake of ^{89}Zr-DNP was observsed in macrophage-rich plaques in a murine model. Moreover, the signal decreased using a siRNA targeted to CCR2, which is a monocytes/macrophages recruitment marker [133]. Perez-Medina et al. developed a discoidal high-density lipoprotein (HDL) nanoparticle. After labeling with ^{89}Zr or using near-infrared fluorescence, the HDL-NP was found to migrate to macrophage-rich plaques in three atherosclerotic models (mice, rabbit and pig). Since HDL is a natural material removes cholesterol from plaque, HDL-NP has promise for clinical translation [134]. Another biocompatible material used for in vivo imaging is hyaluronan (HA), which is a component of extracellular matrix and has diverse biological activities. Recently, ^{89}Zr/Cy7 labeled hyaluronan nanoparticles (HA-NPs) showed 30% higher accumulation in the aortas of a atherosclerotic model mice compared to controls using PET/MR imaging. The Cy7-HA-NPs displayed a 6 to 40-fold uptake increase in aortic macrophages compared to normal tissue macrophages. In addition, the HA-NPs exhibited immune modulation effects that inhibited disease progression [135]. LyP-1 is a cyclic 9-amino acid peptide that binds with the p32 protein on activated macrophages. Seo et al. improved the dectection of macrophages using LyP-1 decorated dendritic NPs compared to ^{18}F labeled single LyP-1 imaging [136]. Ni et al. described a ^{64}Cu-folate-porphysome, a bilayered nanovesicle self-assembled from phospholipid-porphyrin conjugates, for tracking macrophages after myocardial infarction. After decoration with folate on the surface and radiolabeled with ^{64}Cu, the PET results showed that ^{64}Cu-folate-porphysome accumulated at infarct sites on days 2 and 7. However, ^{64}Cu-porphysome without folate modification did not [137].

Compared with ^{89}Zr and ^{64}Cu, ^{18}F is more suitable in the clinic since there is less radiation exposure from a short half-life. ^{18}F radiolabel NPs have recently drawn attention in PET imaging. Based on a pre-targeting strategy, Jeong et al. investigated the feasibility of ^{18}F-labeledmesoporous silica NPs (DBCO-MSNs) for tracking macrophages migration in atherosclerosis model and tumor model. DBCO-MSNs and macrophages were incubated in vitro and then injected into model mice. After 1-8 days, [^{18}F]2 was intravenously injected for DBCO-MSNs labeling. After PET imaging, atherosclerotic mice injected with DBCO-MSNs-RAW cells showed higher SUVs in aortas than the mice injected with normal RAW cells, which were supported by autoradiography and immunostaining. These results indicate pre-targeting with DBCO-MSNs is feasible for tracking macrophages in an atherosclerotic model [138]. Keliher and colleagues reported small modified-polyglucose NPs (^{18}F-Macroflor, 5.0 nm diameter), which displayed a high avidity for macrophage. Since the size of NPs were below the renal elimination threshold, they were eliminated from the kidneys and had a short circulating time (only 21.7 min in healthy non-human primate). The small size and short circulating time made Macroflor suitablefor labeling with short half-life isotopes such as ^{18}F. The ^{18}F-Macroflor was then successfully applied for imaging of macrophage-rich plaques in mice and ribbit models (**Figure 2D**) and injured heart tissue in a myocardial infarction mice model (**Figure 2E**). Flow cytometry gating on isolated cells from aortic or infarcted tissues verified the NP was primarily taken up by macrophages but not by neutrophils or lymphocytes. The clinically suitable radioisotope, natural material, and facile click labeling made the ^{18}F-Macroflor highly promising for clinical translation [139] (**Table 2**).

Other potential targets

Inducible nitric oxide synthase (iNOS) is a crucial enzyme that generates large amounts of NO when induced by inflammatory stimuli. Studies have shown that iNOS is highly upregulated in activated M1 macrophages and can therefore be exploited for targeted macrophage imaging [140]. ^{18}F-NOS was developed in 2009 and has successfully been used for PET imaging of iNOS in models of lung inflammation [141, 142]. Moreover, increased ^{18}F-NOS was reported in patients with organ rejection after heart transplantation surgery. The myocardial ^{18}F-NOS uptake also correlated with iNOS staining in heart tissue [143].

Formyl peptide receptor 1 (Fpr1) belongs to the G-protein-coupled receptor family. Expression of Fpr1 has been reported on activated macrophages and other leukocytes. A previous study

Table 3. Summary of other potential targets illustrated in the present review

Target	Disease	Preclinical/clinical	Radiotracer
iNOS	Acute lung inflammation	Clinical	^{18}F-NOS [141, 142]
	Heart transplantation	Clinical	^{18}F-NOS [143]
Fpr1	Osteoarthritis	Preclinical	cFLFLF-PEG-^{64}Cu [144]
CRIg	Rheumatoid arthritis	Preclinical	^{99m}Tc-NbV4m119 [146]
CD80	Atherosclerosis	Preclinical	^{11}C-AM7 [147, 148]
CD163	Collagen-induced arthritis	Preclinical	^{68}Ga-ED2 [149]
CD11b	Cancer	Preclinical	^{64}Cu-NOTA-αCD11b-mAb [150]; ^{89}Zr-anti-CD11b Ab [151]
	Inflamed ear/IBD/Atherosclerosis	Preclinical	^{64}Cu-αCD11b [152]; ^{89}Zr-α-CD11b [153]; ^{99m}Tc-anti-CD11b [154]
CD169	Allograft rejection	Preclinical	^{99m}Tc-SER-4 [155]
CD68	Atherosclerosis	Preclinical	^{64}Cu-CD68-Fc [157]
F4/80	Breast tumor	Preclinical	^{111}In-anti-F4/80-A3-1 [156]

labeled a Fpr1 specific binding peptide (cinnamoyl-F-(D)L-F-(D)L-F) with ^{64}Cu for PET imaging of infiltrating macrophages in osteoarthritic rats. The diseased knee displayed approximately a 6-fold increase compared to its contralateral healthy knee. The tissue and cell lines staining indicated the expression of Fpr1 expressed on macrophages and synovial membranes [144].

Complement receptor of the immunoglobulin superfamily (CRIg) is expressed on tissue-resident macrophages and has an affinity for C3b and iC3b, which can clear probes tagged with C3b and iC3b [145]. Zhang et al. reported a nanobody targeting CRIg for SPECT imaging. ^{99m}Tc-NbV4m119 accumulated in arthritic lesions of the inflamed murine paws. Immunofluorescence staining verified the co-localization of CRIg and CD68$^+$ macrophages in inflamed knee synovium tissue [146].

Several CD markers on macrophages have been identified, which also hold potential to detect macrophages in CVDs using PET imaging. However, to date, most probes targeted these CD markers were antibody-based and mainly investigated in tumor models or other inflammatory related diseases. We will highlight all of these studies irrespective of the modality and disease type. The targets included CD80, CD163, CD11b, CD169, CD68 and F4/80.

The co-stimulatory molecules CD80 and CD86 were found on M1 macrophages in human atherosclerotic plaque and more so in vulnerable plaques [147]. Muller et al. synthesized ^{11}C-AM7, a CD80-specific radiotracer, and showed 3-fold higher binding to vulnerable human plaques compared to stable plaques ex vivo [147]. The ^{11}C-AM7 PET imaging was further proved in a shear stress-induced atherosclerosis mouse model [148]. CD163 is a scavenger receptor for removing plasma hemoglobin during intravascular hemolysis. It has been found to be highly expressed on monocytes and macrophages, particularly M2 macrophages. Eichendorff et al. radiolabeled a CD163 antibody (ED2) with ^{68}Ga and found that it could specifically bind to the CD163 receptor in vitro. Additionally, ^{68}Ga-ED2 accumulated in macrophage-rich tissues of collagen-induced arthritis rat [149]. CD11b, also known as Mac-1, is expressed on macrophage and other leucocytes. Over the years, several radiolabeled anti-CD11b antibody tracers have been investigated in tumor or inflammatory models, including ^{64}Cu-NOTA-αCD11b-mAb in breast and melanoma tumor [150], ^{89}Zr-anti-CD11b Ab in glioblastoma [151], ^{64}Cu-αCD11b in chronic ear inflammation [152], ^{89}Zr-α-CD11b in inflammatory bowel disease (IBD) [153], and ^{99m}Tc-MAG_3-anti-CD11b in atherosclerosis [154]. ^{99m}Tc-SER-4 is a SPECT probe targeting CD169 (sialoadhesin, Sn) and was recently developed to monitor macrophages in chronic transplant rejection [155]. As a pan-macrophages marker in murine model, an F4/80 receptor targeted antibody was applied for imaging tumor-associated macrophages by labeling with ^{111}In. In a murine breast cancer model, the ^{111}In-anti-F4/80-A3-1 uptake was prominate in the tumor and spleen and decreased after clodronate treatment [156]. CD68 is another scavenger receptor on macrophages and is involved in the uptake of modified low-density lipoproteins thereby promoting the formation of foam cells. Thus, an

anti-CD68 PET tracer (^{64}Cu-CD68-Fc) may help monitor plaque development [157] (**Table 3**).

Conclusions and future perspectives

Since the cardiovascular system so vital and well protected, biopsies are risky and challenging. Thus, noninvasive PET imaging has immense potential to provide diagnostic information, particularly when integrated with the soft-tissue contrast of MRI. In vivo tracking of macrophages will benefit both basic research and clinical decision making for CVDs. Revealing macrophages function in CVDs may permit early detection of atherosclerosis or discrimination of unstable plaques. In turn, this can decrease risk of MI or stroke, facilitate the diagnosis of inflammatory cardiomyopathies, and enable monitoring of anti-inflammatory therapies in CVDs.

Over the past 15 years, over 50 macrophage-targeted probes have been described and studied. Among them, metabolism or proliferation-based tracers, including ^{18}F-FDG, ^{11}C-methionine, ^{11}C-Choline, ^{18}F-FCH and ^{18}F-FLT, are nonspecific radiotracers, which seem inferior to specific target-based probes. However, in view of current positive clinical results, the clinical value for diagnosis and therapy monitoring using these probes should not be ignored despite their nonspecific nature.

Additional clinical and comparative studies are required the probes currently developed, particularly those with promising animal study results. To date, including the metabolism- and proliferation-based tracers, 13 probes in have been clinically investigated, including ^{68}Ga-pentixafor, ^{68}Ga-DOTA-TOC, ^{68}Ga-DOTA-NOC, ^{68}Ga-DOTA-TATE, ^{64}Cu-DOTA-TATE, ^{11}C-PK111-95, ^{18}F-GE-180 and ^{18}F-NOS. Unfortunately, most of them involved a small number of patients, were single-center, and retrospective studies. More multi-center and prospective clinical studies would help determine the clinical feasibility and effectiveness of these tracers. Moreover, comparative studies are still lacking. While difficult to compare because different targets may reflect various aspects of macrophage function or the nonspecifity of FDG, additional characteristic information of each tracer would be provide. Furthermore, there are still several available tracers that have not been fully exploited in CVDs. Antibody-based probes are an example that have been developed for PET and SPECT imaging in cancer and other inflammatory diseases but not investigated in CVDs. Thus, antibody probes may hold promising for CVDs in the future.

Next generation probes can be developed by modifying the chemical structure those that already exist. Current probes are not all perfect; thus, modifying the chemical structure to balance the hydrophile or lipophilia may improve probes' performance. Alternatively, developing new targets and novel tracers are still appealing. Each target reflects just one of macrophage functions and not all patients may respond effectively to one tracer. Previous studies have reported positive imaging in some patients but not in the others, which may be ascribed to different receptor expression levels among individuals. Hence, novel targets and tracers with high specificity and generally expression are helpful. Apart from diagnosis, tracers for therapy or theranostic are another promising direction. Early diagnosis would aid in the early prevention of CVDs. Therapy or theranostic tracers would help drug release for modulating macrophages polarization and also treatment monitoring. To this end, NPs are an excellent choice due to the versatile properties that facilitate drug loading and imaging applications.

Target specificity is an essential aspect of imaging studies. Most of studies discussed in this review generally used a comparison between immunohistochemical staining for CD68$^+$ and autoradiography to verify the tracers' specificity for macrophages. While this strategy is useful, it is not comprehensive. This comparison does not provide information about the contribution from other cells to the signal. While finding an absolutely pure target is challenging, the specificity of a tracer clarifies what the signal is truly reflecting. Flow cytometric gating on cells derived from target tissues has been applied in some reports, which may helpful to overcome this concern.

Distinguishing macrophage subtypes with precision is challenging. Generally, two or three cell markers are required to verify M1 or M2 macrophages using flow cytometry, which is difficult for with single-targeted PET imaging. Additionally, M1 and M2 macrophage phenotypes are not stable and can change in response to environmental signals. Although

some targets are reported to be preferably expressed on M2 or M1 macrophages, the specificity is not entirely clear, which makes imaging of macrophage subtypes difficult.

PET imaging of macrophages have been designed to target and image one aspect of macrophages. PET imaging of macrophages in CVDs have distinct advantages for patient diagnosis and can inform treatment decisions. Future work will help us understand the role of macrophages in CVDs and ultimately benefit patients.

Acknowledgements

This study was funded by The National Natural Science Foundation of China (Grant Nos. 91959208, 81971646), The University of Wisconsin-Madison, The National Institutes of Health (P30CA014520).

Disclosure of conflict of interest

None.

Address correspondence to: Dr. Weibo Cai, Department of Radiology and Medical Physics, University of Wisconsin-Madison, Room 7137, 1111 Highland Avenue, Madison, WI 53705-2275, USA. E-mail: wcai@uwhealth.org; Dr. Jing Wang, Department of Nuclear Medicine, Xijing Hospital, Fourth Military Medical University, Xi'an 710032, Shaanxi, China. E-mail: wangjing@fmmu.edu.cn

References

[1] Joseph P, Leong D, McKee M, Anand SS, Schwalm JD, Teo K, Mente A and Yusuf S. Reducing the global burden of cardiovascular disease, part 1: the epidemiology and risk factors. Circ Res 2017; 121: 677-694.

[2] Benjamin EJ, Muntner P, Alonso A, Bittencourt MS, Callaway CW, Carson AP, Chamberlain AM, Chang AR, Cheng S, Das SR, Delling FN, Djousse L, Elkind MSV, Ferguson JF, Fornage M, Jordan LC, Khan SS, Kissela BM, Knutson KL, Kwan TW, Lackland DT, Lewis TT, Lichtman JH, Longenecker CT, Loop MS, Lutsey PL, Martin SS, Matsushita K, Moran AE, Mussolino ME, O'Flaherty M, Pandey A, Perak AM, Rosamond WD, Roth GA, Sampson UKA, Satou GM, Schroeder EB, Shah SH, Spartano NL, Stokes A, Tirschwell DL, Tsao CW, Turakhia MP, VanWagner LB, Wilkins JT, Wong SS and Virani SS; American Heart Association Council on Epidemiology and Prevention Statistics Committee and Stroke Statistics Subcommittee. Heart disease and stroke statistics-2019 update: a report from the american heart association. Circulation 2019; 139: e56-e528.

[3] Hansson GK. Inflammation, atherosclerosis, and coronary artery disease. N Engl J Med 2005; 352: 1685-1695.

[4] Chinetti-Gbaguidi G, Colin S and Staels B. Macrophage subsets in atherosclerosis. Nat Rev Cardiol 2015; 12: 10-17.

[5] Moore KJ and Tabas I. Macrophages in the pathogenesis of atherosclerosis. Cell 2011; 145: 341-355.

[6] Moore KJ, Sheedy FJ and Fisher EA. Macrophages in atherosclerosis: a dynamic balance. Nat Rev Immunol 2013; 13: 709-721.

[7] Koelwyn GJ, Corr EM, Erbay E and Moore KJ. Regulation of macrophage immunometabolism in atherosclerosis. Nat Immunol 2018; 19: 526-537.

[8] Ley K, Miller YI and Hedrick CC. Monocyte and macrophage dynamics during atherogenesis. Arterioscler Thromb Vasc Biol 2011; 31: 1506-1516.

[9] Tabas I and Bornfeldt KE. Macrophage phenotype and function in different stages of atherosclerosis. Circ Res 2016; 118: 653-667.

[10] Virmani R, Burke AP, Kolodgie FD and Farb A. Vulnerable plaque: the pathology of unstable coronary lesions. J Interv Cardiol 2002; 15: 439-446.

[11] Tabas I. The role of endoplasmic reticulum stress in the progression of atherosclerosis. Circ Res 2010; 107: 839-850.

[12] Johnson JL. Metalloproteinases in atherosclerosis. Eur J Pharmacol 2017; 816: 93-106.

[13] Bentzon JF, Otsuka F, Virmani R and Falk E. Mechanisms of plaque formation and rupture. Circ Res 2014; 114: 1852-1866.

[14] O'Rourke SA, Dunne A and Monaghan MG. The role of macrophages in the infarcted myocardium: orchestrators of ECM remodeling. Front Cardiovasc Med 2019; 6: 101.

[15] Lavine KJ, Pinto AR, Epelman S, Kopecky BJ, Clemente-Casares X, Godwin J, Rosenthal N and Kovacic JC. The macrophage in cardiac homeostasis and disease: JACC macrophage in CVD series (part 4). J Am Coll Cardiol 2018; 72: 2213-2230.

[16] Williams JW, Giannarelli C, Rahman A, Randolph GJ and Kovacic JC. Macrophage biology, classification, and phenotype in cardiovascular disease: JACC macrophage in CVD series (part 1). J Am Coll Cardiol 2018; 72: 2166-2180.

[17] Serei VD and Fyfe B. The many faces of cardiac sarcoidosis. Am J Clin Pathol 2020; 153: 294-302.

[18] Heymans S, Eriksson U, Lehtonen J and Cooper LT Jr. The quest for new approaches in myocar-

ditis and inflammatory cardiomyopathy. J Am Coll Cardiol 2016; 68: 2348-2364.
[19] Iung B and Duval X. Infective endocarditis: innovations in the management of an old disease. Nat Rev Cardiol 2019; 16: 623-635.
[20] Jiemy WF, Heeringa P, Kamps J, van der Laken CJ, Slart R and Brouwer E. Positron emission tomography (PET) and single photon emission computed tomography (SPECT) imaging of macrophages in large vessel vasculitis: current status and future prospects. Autoimmun Rev 2018; 17: 715-726.
[21] Dobrucki LW and Sinusas AJ. PET and SPECT in cardiovascular molecular imaging. Nat Rev Cardiol 2010; 7: 38-47.
[22] Jivraj N, Phinikaridou A, Shah AM and Botnar RM. Molecular imaging of myocardial infarction. Basic Res Cardiol 2014; 109: 397.
[23] Garcia EV. Physical attributes, limitations, and future potential for PET and SPECT. J Nucl Cardiol 2012; 19 Suppl 1: S19-29.
[24] Wilk B, Wisenberg G, Dharmakumar R, Thiessen JD, Goldhawk DE and Prato FS. Hybrid PET/MR imaging in myocardial inflammation post-myocardial infarction. J Nucl Cardiol 2019; [Epub ahead of print].
[25] Pimlott SL and Sutherland A. Molecular tracers for the PET and SPECT imaging of disease. Chem Soc Rev 2011; 40: 149-162.
[26] Li Z and Conti PS. Radiopharmaceutical chemistry for positron emission tomography. Adv Drug Deliv Rev 2010; 62: 1031-1051.
[27] Chen K and Conti PS. Target-specific delivery of peptide-based probes for PET imaging. Adv Drug Deliv Rev 2010; 62: 1005-1022.
[28] Kircher M and Lapa C. Novel noninvasive nuclear medicine imaging techniques for cardiac inflammation. Curr Cardiovasc Imaging Rep 2017; 10: 6.
[29] Millar BC, Prendergast BD, Alavi A and Moore JE. 18FDG-positron emission tomography (PET) has a role to play in the diagnosis and therapy of infective endocarditis and cardiac device infection. Int J Cardiol 2013; 167: 1724-1736.
[30] Blomberg BA and Hoilund-Carlsen PF. [(1)(8)F]-fluorodeoxyglucose PET imaging of atherosclerosis. PET Clin 2015; 10: 1-7.
[31] Ali A and Tawakol A. FDG PET/CT imaging of carotid atherosclerosis. Neuroimaging Clin N Am 2016; 26: 45-54.
[32] Bengel FM. Imaging of post-infarct inflammation: moving forward toward clinical application. Circ Cardiovasc Imaging 2016; 9: e004713.
[33] Fox JJ and Strauss HW. One step closer to imaging vulnerable plaque in the coronary arteries. J Nucl Med 2009; 50: 497-500.
[34] Huet P, Burg S, Le Guludec D, Hyafil F and Buvat I. Variability and uncertainty of 18F-FDG PET imaging protocols for assessing inflammation in atherosclerosis: suggestions for improvement. J Nucl Med 2015; 56: 552-559.
[35] Leung K. l-[methyl-(11)C]Methionine. In: editors. Molecular imaging and contrast agent database (MICAD). Bethesda (MD): National Center for Biotechnology Information (US); 2004. pp.
[36] Morooka M, Kubota K, Kadowaki H, Ito K, Okazaki O, Kashida M, Mitsumoto T, Iwata R, Ohtomo K and Hiroe M. 11C-methionine PET of acute myocardial infarction. J Nucl Med 2009; 50: 1283-1287.
[37] Taki J, Wakabayashi H, Inaki A, Imanaka-Yoshida K, Hiroe M, Ogawa K, Morooka M, Kubota K, Shiba K, Yoshida T and Kinuya S. 14C-Methionine uptake as a potential marker of inflammatory processes after myocardial ischemia and reperfusion. J Nucl Med 2013; 54: 431-436.
[38] Thackeray JT, Bankstahl JP, Wang Y, Wollert KC and Bengel FM. Targeting amino acid metabolism for molecular imaging of inflammation early after myocardial infarction. Theranostics 2016; 6: 1768-1779.
[39] Maya Y, Werner RA, Schutz C, Wakabayashi H, Samnick S, Lapa C, Zechmeister C, Jahns R, Jahns V and Higuchi T. 11C-Methionine PET of myocardial inflammation in a rat model of experimental autoimmune myocarditis. J Nucl Med 2016; 57: 1985-1990.
[40] DeGrado TR, Baldwin SW, Wang S, Orr MD, Liao RP, Friedman HS, Reiman R, Price DT and Coleman RE. Synthesis and evaluation of (18) F-labeled choline analogs as oncologic PET tracers. J Nucl Med 2001; 42: 1805-1814.
[41] Kato K, Schober O, Ikeda M, Schafers M, Ishigaki T, Kies P, Naganawa S and Stegger L. Evaluation and comparison of 11C-choline uptake and calcification in aortic and common carotid arterial walls with combined PET/CT. Eur J Nucl Med Mol Imaging 2009; 36: 1622-1628.
[42] Laitinen IE, Luoto P, Nagren K, Marjamaki PM, Silvola JM, Hellberg S, Laine VJ, Yla-Herttuala S, Knuuti J and Roivainen A. Uptake of 11C-choline in mouse atherosclerotic plaques. J Nucl Med 2010; 51: 798-802.
[43] Matter CM, Wyss MT, Meier P, Spath N, von Lukowicz T, Lohmann C, Weber B, Ramirez de Molina A, Lacal JC, Ametamey SM, von Schulthess GK, Luscher TF, Kaufmann PA and Buck A. 18F-choline images murine atherosclerotic plaques ex vivo. Arterioscler Thromb Vasc Biol 2006; 26: 584-589.
[44] Bucerius J, Schmaljohann J, Bohm I, Palmedo H, Guhlke S, Tiemann K, Schild HH, Biersack HJ and Manka C. Feasibility of 18F-fluoromethylcholine PET/CT for imaging of ves-

sel wall alterations in humans--first results. Eur J Nucl Med Mol Imaging 2008; 35: 815-820.
[45] Vöö S, Kwee RM, Sluimer JC, Schreuder FH, Wierts R, Bauwens M, Heeneman S, Cleutjens JP, van Oostenbrugge RJ, Daemen JW, Daemen MJ, Mottaghy FM and Kooi ME. Imaging intraplaque inflammation in carotid atherosclerosis with 18F-fluorocholine positron emission tomography-computed tomography: prospective study on vulnerable atheroma with immunohistochemical validation. Circ Cardiovasc Imaging 2016; 9.
[46] Leung K. 3'-Deoxy-3''-[(18)F]fluorothymidine. In: editors. Molecular imaging and contrast agent database (MICAD). Bethesda (MD): National Center for Biotechnology Information (US); 2004. pp.
[47] Ye YX, Calcagno C, Binderup T, Courties G, Keliher EJ, Wojtkiewicz GR, Iwamoto Y, Tang J, Perez-Medina C, Mani V, Ishino S, Johnbeck CB, Knigge U, Fayad ZA, Libby P, Weissleder R, Tawakol A, Dubey S, Belanger AP, Di Carli MF, Swirski FK, Kjaer A, Mulder WJ and Nahrendorf M. Imaging macrophage and hematopoietic progenitor proliferation in atherosclerosis. Circ Res 2015; 117: 835-845.
[48] Gandhi R, Cawthorne C, Craggs LJL, Wright JD, Domarkas J, He P, Koch-Paszkowski J, Shires M, Scarsbrook AF, Archibald SJ, Tsoumpas C and Bailey MA. Cell proliferation detected using [(18)F]FLT PET/CT as an early marker of abdominal aortic aneurysm. J Nucl Cardiol 2019; [Epub ahead of print].
[49] Rajagopalan L and Rajarathnam K. Structural basis of chemokine receptor function--a model for binding affinity and ligand selectivity. Biosci Rep 2006; 26: 325-339.
[50] Schwarz MK and Wells TN. New therapeutics that modulate chemokine networks. Nat Rev Drug Discov 2002; 1: 347-358.
[51] van der Vorst EP, Doring Y and Weber C. Chemokines and their receptors in atherosclerosis. J Mol Med (Berl) 2015; 93: 963-971.
[52] Doring Y, Pawig L, Weber C and Noels H. The CXCL12/CXCR4 chemokine ligand/receptor axis in cardiovascular disease. Front Physiol 2014; 5: 212.
[53] Kolattukudy PE and Niu J. Inflammation, endoplasmic reticulum stress, autophagy, and the monocyte chemoattractant protein-1/CCR2 pathway. Circ Res 2012; 110: 174-189.
[54] Zhao Q. Dual targeting of CCR2 and CCR5: therapeutic potential for immunologic and cardiovascular diseases. J Leukoc Biol 2010; 88: 41-55.
[55] Wester HJ, Keller U, Schottelius M, Beer A, Philipp-Abbrederis K, Hoffmann F, Simecek J, Gerngross C, Lassmann M, Herrmann K, Pellegata N, Rudelius M, Kessler H and Schwaiger M. Disclosing the CXCR4 expression in lymphoproliferative diseases by targeted molecular imaging. Theranostics 2015; 5: 618-630.
[56] Kircher M, Herhaus P, Schottelius M, Buck AK, Werner RA, Wester HJ, Keller U and Lapa C. CXCR4-directed theranostics in oncology and inflammation. Ann Nucl Med 2018; 32: 503-511.
[57] Thackeray JT, Derlin T, Haghikia A, Napp LC, Wang Y, Ross TL, Schafer A, Tillmanns J, Wester HJ, Wollert KC, Bauersachs J and Bengel FM. Molecular imaging of the chemokine receptor CXCR4 after acute myocardial infarction. JACC Cardiovasc Imaging 2015; 8: 1417-1426.
[58] Lapa C, Reiter T, Werner RA, Ertl G, Wester HJ, Buck AK, Bauer WR and Herrmann K. [(68)Ga]Pentixafor-PET/CT for Imaging of Chemokine Receptor 4 expression after myocardial infarction. JACC Cardiovasc Imaging 2015; 8: 1466-1468.
[59] Reiter T, Kircher M, Schirbel A, Werner RA, Kropf S, Ertl G, Buck AK, Wester HJ, Bauer WR and Lapa C. Imaging of C-X-C Motif chemokine receptor CXCR4 expression after myocardial infarction with [(68)Ga]pentixafor-PET/CT in correlation with cardiac MRI. JACC Cardiovasc Imaging 2018; 11: 1541-1543.
[60] Hyafil F, Pelisek J, Laitinen I, Schottelius M, Mohring M, Doring Y, van der Vorst EP, Kallmayer M, Steiger K, Poschenrieder A, Notni J, Fischer J, Baumgartner C, Rischpler C, Nekolla SG, Weber C, Eckstein HH, Wester HJ and Schwaiger M. Imaging the cytokine receptor CXCR4 in atherosclerotic plaques with the radiotracer (68)Ga-Pentixafor for PET. J Nucl Med 2017; 58: 499-506.
[61] Weiberg D, Thackeray JT, Daum G, Sohns JM, Kropf S, Wester HJ, Ross TL, Bengel FM and Derlin T. Clinical molecular imaging of chemokine receptor CXCR4 expression in atherosclerotic plaque using (68)Ga-Pentixafor PET: correlation with cardiovascular risk factors and calcified plaque burden. J Nucl Med 2018; 59: 266-272.
[62] Li X, Heber D, Leike T, Beitzke D, Lu X, Zhang X, Wei Y, Mitterhauser M, Wadsak W, Kropf S, Wester HJ, Loewe C, Hacker M and Haug AR. [68Ga]Pentixafor-PET/MRI for the detection of Chemokine receptor 4 expression in atherosclerotic plaques. Eur J Nucl Med Mol Imaging 2018; 45: 558-566.
[63] Li X, Yu W, Wollenweber T, Lu X, Wei Y, Beitzke D, Wadsak W, Kropf S, Wester HJ, Haug AR, Zhang X and Hacker M. [(68)Ga]Pentixafor PET/MR imaging of chemokine receptor 4 expression in the human carotid artery. Eur J Nucl Med Mol Imaging 2019; 46: 1616-1625.
[64] Kircher M, Tran-Gia J, Kemmer L, Zhang X, Schirbel A, Werner RA, Buck AK, Wester HJ,

Hacker M, Lapa C and Li X. Imaging inflammation in atherosclerosis with CXCR4-directed (68)Ga-Pentixafor PET/CT - correlation with (18)F-FDG PET/CT. J Nucl Med 2019; [Epub ahead of print].

[65] Derlin T, Sedding DG, Dutzmann J, Haghikia A, Konig T, Napp LC, Schutze C, Owsianski-Hille N, Wester HJ, Kropf S, Thackeray JT, Bankstahl JP, Geworski L, Ross TL, Bauersachs J and Bengel FM. Imaging of chemokine receptor CXCR4 expression in culprit and nonculprit coronary atherosclerotic plaque using motion-corrected [(68)Ga]pentixafor PET/CT. Eur J Nucl Med Mol Imaging 2018; 45: 1934-1944.

[66] Auvynet C, Baudesson de Chanville C, Hermand P, Dorgham K, Piesse C, Pouchy C, Carlier L, Poupel L, Barthelemy S, Felouzis V, Lacombe C, Sagan S, Chemtob S, Quiniou C, Salomon B, Deterre P, Sennlaub F and Combadiere C. ECL1i, d(LGTFLKC), a novel, small peptide that specifically inhibits CCL2-dependent migration. FASEB J 2016; 30: 2370-2381.

[67] Liu Y, Li W, Luehmann HP, Zhao Y, Detering L, Sultan DH, Hsiao HM, Krupnick AS, Gelman AE, Combadiere C, Gropler RJ, Brody SL and Kreisel D. Noninvasive Imaging of CCR2(+) cells in ischemia-reperfusion injury after lung transplantation. Am J Transplant 2016; 16: 3016-3023.

[68] Liu Y, Gunsten SP, Sultan DH, Luehmann HP, Zhao Y, Blackwell TS, Bollermann-Nowlis Z, Pan JH, Byers DE, Atkinson JJ, Kreisel D, Holtzman MJ, Gropler RJ, Combadiere C and Brody SL. PET-based imaging of chemokine receptor 2 in experimental and disease-related lung inflammation. Radiology 2017; 283: 758-768.

[69] Heo GS, Kopecky B, Sultan D, Ou M, Feng G, Bajpai G, Zhang X, Luehmann H, Detering L, Su Y, Leuschner F, Combadiere C, Kreisel D, Gropler RJ, Brody SL, Liu Y and Lavine KJ. Molecular imaging visualizes recruitment of inflammatory monocytes and macrophages to the injured heart. Circ Res 2019; 124: 881-890.

[70] Liu Y, Pierce R, Luehmann HP, Sharp TL and Welch MJ. PET imaging of chemokine receptors in vascular injury-accelerated atherosclerosis. J Nucl Med 2013; 54: 1135-1141.

[71] Luehmann HP, Pressly ED, Detering L, Wang C, Pierce R, Woodard PK, Gropler RJ, Hawker CJ and Liu Y. PET/CT imaging of chemokine receptor CCR5 in vascular injury model using targeted nanoparticle. J Nucl Med 2014; 55: 629-634.

[72] Luehmann HP, Detering L, Fors BP, Pressly ED, Woodard PK, Randolph GJ, Gropler RJ, Hawker CJ and Liu Y. PET/CT imaging of chemokine receptors in inflammatory atherosclerosis using targeted nanoparticles. J Nucl Med 2016; 57: 1124-1129.

[73] Weckbecker G, Lewis I, Albert R, Schmid HA, Hoyer D and Bruns C. Opportunities in somatostatin research: biological, chemical and therapeutic aspects. Nat Rev Drug Discov 2003; 2: 999-1017.

[74] Leung K. (68)Ga-1,4,7,10-Tetraazacyclododecane-1,4,7,10-tetraacetic acid-Cpa-cyclo(d-Cys-amino-Phe-hydroorotic acid-D-4-amino-Phe(carbamoyl)-Lys-Thr-Cys)-D-Tyr-NH2 (JR11). In: editors. Molecular imaging and contrast agent database (MICAD). Bethesda (MD): National Center for Biotechnology Information (US); 2004. pp.

[75] Li X, Bauer W, Kreissl MC, Weirather J, Bauer E, Israel I, Richter D, Riehl G, Buck A and Samnick S. Specific somatostatin receptor II expression in arterial plaque: (68)Ga-DOTATATE autoradiographic, immunohistochemical and flow cytometric studies in apoE-deficient mice. Atherosclerosis 2013; 230: 33-39.

[76] Rominger A, Saam T, Vogl E, Ubleis C, la Fougere C, Forster S, Haug A, Cumming P, Reiser MF, Nikolaou K, Bartenstein P and Hacker M. In vivo imaging of macrophage activity in the coronary arteries using 68Ga-DOTATATE PET/CT: correlation with coronary calcium burden and risk factors. J Nucl Med 2010; 51: 193-197.

[77] Li X, Samnick S, Lapa C, Israel I, Buck AK, Kreissl MC and Bauer W. 68Ga-DOTATATE PET/CT for the detection of inflammation of large arteries: correlation with18F-FDG, calcium burden and risk factors. EJNMMI Res 2012; 2: 52.

[78] Mojtahedi A, Alavi A, Thamake S, Amerinia R, Ranganathan D, Tworowska I and Delpassand ES. Assessment of vulnerable atherosclerotic and fibrotic plaques in coronary arteries using (68)Ga-DOTATATE PET/CT. Am J Nucl Med Mol Imaging 2015; 5: 65-71.

[79] Rinne P, Hellberg S, Kiugel M, Virta J, Li XG, Kakela M, Helariutta K, Luoto P, Liljenback H, Hakovirta H, Gardberg M, Airaksinen AJ, Knuuti J, Saraste A and Roivainen A. Comparison of somatostatin receptor 2-targeting PET tracers in the detection of mouse atherosclerotic plaques. Mol Imaging Biol 2016; 18: 99-108.

[80] Malmberg C, Ripa RS, Johnbeck CB, Knigge U, Langer SW, Mortensen J, Oturai P, Loft A, Hag AM and Kjaer A. 64Cu-DOTATATE for noninvasive assessment of atherosclerosis in large arteries and its correlation with risk factors: head-to-head comparison with 68Ga-DOTATOC in 60 patients. J Nucl Med 2015; 56: 1895-1900.

[81] Pedersen SF, Sandholt BV, Keller SH, Hansen AE, Clemmensen AE, Sillesen H, Hojgaard L,

Ripa RS and Kjaer A. 64Cu-DOTATATE PET/MRI for detection of activated macrophages in carotid atherosclerotic plaques: studies in patients undergoing endarterectomy. Arterioscler Thromb Vasc Biol 2015; 35: 1696-1703.

[82] Tarkin JM, Joshi FR, Evans NR, Chowdhury MM, Figg NL, Shah AV, Starks LT, Martin-Garrido A, Manavaki R, Yu E, Kuc RE, Grassi L, Kreuzhuber R, Kostadima MA, Frontini M, Kirkpatrick PJ, Coughlin PA, Gopalan D, Fryer TD, Buscombe JR, Groves AM, Ouwehand WH, Bennett MR, Warburton EA, Davenport AP and Rudd JH. Detection of atherosclerotic inflammation by (68)Ga-DOTATATE PET compared to [(18)F]FDG PET imaging. J Am Coll Cardiol 2017; 69: 1774-1791.

[83] Wan MYS, Endozo R, Michopoulou S, Shortman R, Rodriguez-Justo M, Menezes L, Yusuf S, Richards T, Wild D, Waser B, Reubi JC and Groves A. PET/CT imaging of unstable carotid plaque with (68)Ga-labeled somatostatin receptor ligand. J Nucl Med 2017; 58: 774-780.

[84] Reiter T, Werner RA, Bauer WR and Lapa C. Detection of cardiac sarcoidosis by macrophage-directed somatostatin receptor 2-based positron emission tomography/computed tomography. Eur Heart J 2015; 36: 2404.

[85] Lapa C, Reiter T, Kircher M, Schirbel A, Werner RA, Pelzer T, Pizarro C, Skowasch D, Thomas L, Schlesinger-Irsch U, Thomas D, Bundschuh RA, Bauer WR and Gartner FC. Somatostatin receptor based PET/CT in patients with the suspicion of cardiac sarcoidosis: an initial comparison to cardiac MRI. Oncotarget 2016; 7: 77807-77814.

[86] Lapa C, Reiter T, Li X, Werner RA, Samnick S, Jahns R, Buck AK, Ertl G and Bauer WR. Imaging of myocardial inflammation with somatostatin receptor based PET/CT - A comparison to cardiac MRI. Int J Cardiol 2015; 194: 44-49.

[87] Pizarro C, Kluenker F, Dabir D, Thomas D, Gaertner FC, Essler M, Grohe C, Nickenig G and Skowasch D. Cardiovascular magnetic resonance imaging and clinical performance of somatostatin receptor positron emission tomography in cardiac sarcoidosis. ESC Heart Fail 2018; 5: 249-261.

[88] Gormsen LC, Haraldsen A, Kramer S, Dias AH, Kim WY and Borghammer P. A dual tracer (68) Ga-DOTANOC PET/CT and (18)F-FDG PET/CT pilot study for detection of cardiac sarcoidosis. EJNMMI Res 2016; 6: 52.

[89] Bravo PE, Bajaj N, Padera RF, Morgan V, Hainer J, Bibbo CF, Harrington M, Park MA, Hyun H, Robertson M, Lakdawala NK, Groarke J, Stewart GC, Dorbala S, Blankstein R and Di Carli MF. Feasibility of somatostatin receptor-targeted imaging for detection of myocardial inflammation: a pilot study. J Nucl Cardiol 2019; [Epub ahead of print].

[90] Thackeray JT, Bankstahl JP, Wang Y, Korf-Klingebiel M, Walte A, Wittneben A, Wollert KC and Bengel FM. Targeting post-infarct inflammation by PET imaging: comparison of (68)Ga-citrate and (68)Ga-DOTATATE with (18)F-FDG in a mouse model. Eur J Nucl Med Mol Imaging 2015; 42: 317-327.

[91] Leung K. 1-(2-Chlorophenyl)-N-[(11)C]methyl-N-(1-methylpropyl)-3-isoquinoline carboxamide. In: editors. Molecular imaging and contrast agent database (MICAD). Bethesda (MD): National Center for Biotechnology Information (US); 2004. pp.

[92] Denora N and Natile G. An updated view of translocator protein (TSPO). Int J Mol Sci 2017; 18.

[93] Mukherjee S, Sonanini D, Maurer A and Daldrup-Link HE. The Yin and Yang of imaging tumor associated macrophages with PET and MRI. Theranostics 2019; 9: 7730-7748.

[94] Laitinen I, Marjamaki P, Nagren K, Laine VJ, Wilson I, Leppanen P, Yla-Herttuala S, Roivainen A and Knuuti J. Uptake of inflammatory cell marker [11C]PK11195 into mouse atherosclerotic plaques. Eur J Nucl Med Mol Imaging 2009; 36: 73-80.

[95] Tegler G, Sorensen J, Ericson K, Bjorck M and Wanhainen A. 4D-PET/CT with [(11)C]-PK11-195 and [(11)C]-(D)-deprenyl does not identify the chronic inflammation in asymptomatic abdominal aortic aneurysms. Eur J Vasc Endovasc Surg 2013; 45: 351-356.

[96] Gaemperli O, Shalhoub J, Owen DR, Lamare F, Johansson S, Fouladi N, Davies AH, Rimoldi OE and Camici PG. Imaging intraplaque inflammation in carotid atherosclerosis with 11C-PK11195 positron emission tomography/computed tomography. Eur Heart J 2012; 33: 1902-1910.

[97] Cuhlmann S, Gsell W, Van der Heiden K, Habib J, Tremoleda JL, Khalil M, Turkheimer F, Meens MJ, Kwak BR, Bird J, Davenport AP, Clark J, Haskard D, Krams R, Jones H and Evans PC. In vivo mapping of vascular inflammation using the translocator protein tracer 18F-FEDAA1106. Mol Imaging 2014; 13.

[98] Zhang H, Xiao J, Zhou J, Tan H, Hu Y, Mao W, Fu Z, Lin Q, Shi H and Cheng D. 18F-PBR06 PET/CT imaging for evaluating atherosclerotic plaques linked to macrophage infiltration. Nucl Med Commun 2019; 40: 370-376.

[99] Hellberg S, Silvola JMU, Kiugel M, Liljenback H, Savisto N, Li XG, Thiele A, Lehmann L, Heinrich T, Vollmer S, Hakovirta H, Laine VJO, Yla-Herttuala S, Knuuti J, Roivainen A and Saraste A. 18-kDa translocator protein ligand (18) F-FEMPA: biodistribution and uptake into ath-

erosclerotic plaques in mice. J Nucl Cardiol 2017; 24: 862-871.
[100] Hellberg S, Liljenback H, Eskola O, Morisson-Iveson V, Morrison M, Trigg W, Saukko P, Yla-Herttuala S, Knuuti J, Saraste A and Roivainen A. Positron emission tomography imaging of macrophages in atherosclerosis with (18)F-GE-180, a radiotracer for translocator protein (TSPO). Contrast Media Mol Imaging 2018; 2018: 9186902.
[101] Thackeray JT, Hupe HC, Wang Y, Bankstahl JP, Berding G, Ross TL, Bauersachs J, Wollert KC and Bengel FM. Myocardial inflammation predicts remodeling and neuroinflammation after myocardial infarction. J Am Coll Cardiol 2018; 71: 263-275.
[102] Kim GR, Paeng JC, Jung JH, Moon BS, Lopalco A, Denora N, Lee BC and Kim SE. Assessment of TSPO in a rat experimental autoimmune myocarditis model: a comparison study between [(18)F]fluoromethyl-PBR28 and [(18)F] CB251. Int J Mol Sci 2018; 19.
[103] Martinez-Pomares L. The mannose receptor. J Leukoc Biol 2012; 92: 1177-1186.
[104] Tahara N, Mukherjee J, de Haas HJ, Petrov AD, Tawakol A, Haider N, Tahara A, Constantinescu CC, Zhou J, Boersma HH, Imaizumi T, Nakano M, Finn A, Fayad Z, Virmani R, Fuster V, Bosca L and Narula J. 2-deoxy-2-[18F]fluoro-D-mannose positron emission tomography imaging in atherosclerosis. Nat Med 2014; 20: 215-219.
[105] Kim EJ, Kim S, Seo HS, Lee YJ, Eo JS, Jeong JM, Lee B, Kim JY, Park YM and Jeong M. Novel PET Imaging of atherosclerosis with 68Ga-labeled NOTA-neomannosylated human serum albumin. J Nucl Med 2016; 57: 1792-1797.
[106] Senders ML, Hernot S, Carlucci G, van de Voort JC, Fay F, Calcagno C, Tang J, Alaarg A, Zhao Y, Ishino S, Palmisano A, Boeykens G, Meerwaldt AE, Sanchez-Gaytan BL, Baxter S, Zendman L, Lobatto ME, Karakatsanis NA, Robson PM, Broisat A, Raes G, Lewis JS, Tsimikas S, Reiner T, Fayad ZA, Devoogdt N, Mulder WJM and Perez-Medina C. Nanobody-facilitated multiparametric PET/MRI phenotyping of atherosclerosis. JACC Cardiovasc Imaging 2019; 12: 2015-2026.
[107] Varasteh Z, Mohanta S, Li Y, Lopez Armbruster N, Braeuer M, Nekolla SG, Habenicht A, Sager HB, Raes G, Weber W, Hernot S and Schwaiger M. Targeting mannose receptor expression on macrophages in atherosclerotic plaques of apolipoprotein E-knockout mice using (68)Ga-NOTA-anti-MMR nanobody: non-invasive imaging of atherosclerotic plaques. EJNMMI Res 2019; 9: 5.
[108] Lee SP, Im HJ, Kang S, Chung SJ, Cho YS, Kang H, Park HS, Hwang DW, Park JB, Paeng JC, Cheon GJ, Lee YS, Jeong JM and Kim YJ. Noninvasive imaging of myocardial inflammation in myocarditis using (68)Ga-tagged mannosylated human serum albumin positron emission tomography. Theranostics 2017; 7: 413-424.
[109] Lindsey ML. Assigning matrix metalloproteinase roles in ischaemic cardiac remodelling. Nat Rev Cardiol 2018; 15: 471-479.
[110] Lebel R and Lepage M. A comprehensive review on controls in molecular imaging: lessons from MMP-2 imaging. Contrast Media Mol Imaging 2014; 9: 187-210.
[111] Su H, Spinale FG, Dobrucki LW, Song J, Hua J, Sweterlitsch S, Dione DP, Cavaliere P, Chow C, Bourke BN, Hu XY, Azure M, Yalamanchili P, Liu R, Cheesman EH, Robinson S, Edwards DS and Sinusas AJ. Noninvasive targeted imaging of matrix metalloproteinase activation in a murine model of postinfarction remodeling. Circulation 2005; 112: 3157-3167.
[112] Sahul ZH, Mukherjee R, Song J, McAteer J, Stroud RE, Dione DP, Staib L, Papademetris X, Dobrucki LW, Duncan JS, Spinale FG and Sinusas AJ. Targeted imaging of the spatial and temporal variation of matrix metalloproteinase activity in a porcine model of postinfarct remodeling: relationship to myocardial dysfunction. Circ Cardiovasc Imaging 2011; 4: 381-391.
[113] van Duijnhoven SM, Robillard MS, Hermann S, Kuhlmann MT, Schafers M, Nicolay K and Grull H. Imaging of MMP activity in postischemic cardiac remodeling using radiolabeled MMP-2/9 activatable peptide probes. Mol Pharm 2014; 11: 1415-1423.
[114] Kiugel M, Kyto V, Saanijoki T, Liljenback H, Metsala O, Stahle M, Tuomela J, Li XG, Saukko P, Knuuti J, Roivainen A and Saraste A. Evaluation of (68)Ga-labeled peptide tracer for detection of gelatinase expression after myocardial infarction in rat. J Nucl Cardiol 2018; 25: 1114-1123.
[115] Lenglet S, Thomas A, Chaurand P, Galan K, Mach F and Montecucco F. Molecular imaging of matrix metalloproteinases in atherosclerotic plaques. Thromb Haemost 2012; 107: 409-416.
[116] Kiugel M, Hellberg S, Kakela M, Liljenback H, Saanijoki T, Li XG, Tuomela J, Knuuti J, Saraste A and Roivainen A. Evaluation of [(68)Ga]Ga-DOTA-TCTP-1 for the detection of metalloproteinase 2/9 expression in mouse atherosclerotic plaques. Molecules 2018; 23.
[117] Wang C, Keliher E, Zeller MWG, Wojtkiewicz GR, Aguirre AD, Buckbinder L, Kim HY, Chen J, Maresca K, Ahmed MS, Motlagh NJ, Nahrendorf M and Chen JW. An activatable PET imaging radioprobe is a dynamic reporter of myeloperoxidase activity in vivo. Proc Natl Acad Sci U S A 2019; 116: 11966-11971.

[118] Ali M, Pulli B and Chen JW. Molecular imaging of macrophage enzyme activity in cardiac inflammation. Curr Cardiovasc Imaging Rep 2014; 7: 9258.
[119] Mollenhauer M, Friedrichs K, Lange M, Gesenberg J, Remane L, Kerkenpass C, Krause J, Schneider J, Ravekes T, Maass M, Halbach M, Peinkofer G, Saric T, Mehrkens D, Adam M, Deuschl FG, Lau D, Geertz B, Manchanda K, Eschenhagen T, Kubala L, Rudolph TK, Wu Y, Tang WHW, Hazen SL, Baldus S, Klinke A and Rudolph V. Myeloperoxidase mediates postischemic arrhythmogenic ventricular remodeling. Circ Res 2017; 121: 56-70.
[120] Nahrendorf M, Sosnovik D, Chen JW, Panizzi P, Figueiredo JL, Aikawa E, Libby P, Swirski FK and Weissleder R. Activatable magnetic resonance imaging agent reports myeloperoxidase activity in healing infarcts and noninvasively detects the antiinflammatory effects of atorvastatin on ischemia-reperfusion injury. Circulation 2008; 117: 1153-1160.
[121] Ronald JA, Chen JW, Chen Y, Hamilton AM, Rodriguez E, Reynolds F, Hegele RA, Rogers KA, Querol M, Bogdanov A, Weissleder R and Rutt BK. Enzyme-sensitive magnetic resonance imaging targeting myeloperoxidase identifies active inflammation in experimental rabbit atherosclerotic plaques. Circulation 2009; 120: 592-599.
[122] Rashid I, Maghzal GJ, Chen YC, Cheng D, Talib J, Newington D, Ren M, Vajandar SK, Searle A, Maluenda A, Lindstedt EL, Jabbour A, Kettle AJ, Bongers A, Power C, Michaelsson E, Peter K and Stocker R. Myeloperoxidase is a potential molecular imaging and therapeutic target for the identification and stabilization of high-risk atherosclerotic plaque. Eur Heart J 2018; 39: 3301-3310.
[123] Wu MC, Ho HI, Lee TW, Wu HL and Lo JM. In vivo examination of 111In-bis-5HT-DTPA to target myeloperoxidase in atherosclerotic ApoE knockout mice. J Drug Target 2012; 20: 605-614.
[124] Johnstrom P, Bergman L, Varnas K, Malmquist J, Halldin C and Farde L. Development of rapid multistep carbon-11 radiosynthesis of the myeloperoxidase inhibitor AZD3241 to assess brain exposure by PET microdosing. Nucl Med Biol 2015; 42: 555-560.
[125] Stendahl JC and Sinusas AJ. Nanoparticles for cardiovascular imaging and therapeutic delivery, part 1: compositions and features. J Nucl Med 2015; 56: 1469-1475.
[126] Cheng Z, Al Zaki A, Hui JZ, Muzykantov VR and Tsourkas A. Multifunctional nanoparticles: cost versus benefit of adding targeting and imaging capabilities. Science 2012; 338: 903-910.
[127] McCarthy JR. Multifunctional agents for concurrent imaging and therapy in cardiovascular disease. Adv Drug Deliv Rev 2010; 62: 1023-1030.
[128] Xie J, Lee S and Chen X. Nanoparticle-based theranostic agents. Adv Drug Deliv Rev 2010; 62: 1064-1079.
[129] Flannagan RS, Jaumouille V and Grinstein S. The cell biology of phagocytosis. Annu Rev Pathol 2012; 7: 61-98.
[130] Lim JP and Gleeson PA. Macropinocytosis: an endocytic pathway for internalising large gulps. Immunol Cell Biol 2011; 89: 836-843.
[131] Weissleder R, Nahrendorf M and Pittet MJ. Imaging macrophages with nanoparticles. Nat Mater 2014; 13: 125-138.
[132] Nahrendorf M, Zhang H, Hembrador S, Panizzi P, Sosnovik DE, Aikawa E, Libby P, Swirski FK and Weissleder R. Nanoparticle PET-CT imaging of macrophages in inflammatory atherosclerosis. Circulation 2008; 117: 379-387.
[133] Majmudar MD, Yoo J, Keliher EJ, Truelove JJ, Iwamoto Y, Sena B, Dutta P, Borodovsky A, Fitzgerald K, Di Carli MF, Libby P, Anderson DG, Swirski FK, Weissleder R and Nahrendorf M. Polymeric nanoparticle PET/MR imaging allows macrophage detection in atherosclerotic plaques. Circ Res 2013; 112: 755-761.
[134] Perez-Medina C, Binderup T, Lobatto ME, Tang J, Calcagno C, Giesen L, Wessel CH, Witjes J, Ishino S, Baxter S, Zhao Y, Ramachandran S, Eldib M, Sanchez-Gaytan BL, Robson PM, Bini J, Granada JF, Fish KM, Stroes ES, Duivenvoorden R, Tsimikas S, Lewis JS, Reiner T, Fuster V, Kjaer A, Fisher EA, Fayad ZA and Mulder WJ. In vivo PET imaging of HDL in multiple atherosclerosis models. JACC Cardiovasc Imaging 2016; 9: 950-961.
[135] Beldman TJ, Senders ML, Alaarg A, Perez-Medina C, Tang J, Zhao Y, Fay F, Deichmoller J, Born B, Desclos E, van der Wel NN, Hoebe RA, Kohen F, Kartvelishvily E, Neeman M, Reiner T, Calcagno C, Fayad ZA, de Winther MPJ, Lutgens E, Mulder WJM and Kluza E. Hyaluronan nanoparticles selectively target plaque-associated macrophages and improve plaque stability in atherosclerosis. ACS Nano 2017; 11: 5785-5799.
[136] Seo JW, Baek H, Mahakian LM, Kusunose J, Hamzah J, Ruoslahti E and Ferrara KW. (64) Cu-labeled LyP-1-dendrimer for PET-CT imaging of atherosclerotic plaque. Bioconjug Chem 2014; 25: 231-239.
[137] Ni NC, Jin CS, Cui L, Shao Z, Wu J, Li SH, Weisel RD, Zheng G and Li RK. Non-invasive macrophage tracking using novel porphysome nanoparticles in the post-myocardial infarction murine heart. Mol Imaging Biol 2016; 18: 557-568.

[138] Jeong HJ, Yoo RJ, Kim JK, Kim MH, Park SH, Kim H, Lim JW, Do SH, Lee KC, Lee YJ and Kim DW. Macrophage cell tracking PET imaging using mesoporous silica nanoparticles via in vivo bioorthogonal F-18 labeling. Biomaterials 2019; 199: 32-39.

[139] Keliher EJ, Ye YX, Wojtkiewicz GR, Aguirre AD, Tricot B, Senders ML, Groenen H, Fay F, Perez-Medina C, Calcagno C, Carlucci G, Reiner T, Sun Y, Courties G, Iwamoto Y, Kim HY, Wang C, Chen JW, Swirski FK, Wey HY, Hooker J, Fayad ZA, Mulder WJ, Weissleder R and Nahrendorf M. Polyglucose nanoparticles with renal elimination and macrophage avidity facilitate PET imaging in ischaemic heart disease. Nat Commun 2017; 8: 14064.

[140] Anavi S and Tirosh O. iNOS as a metabolic enzyme under stress conditions. Free Radic Biol Med 2020; 146: 16-35.

[141] Zhou D, Lee H, Rothfuss JM, Chen DL, Ponde DE, Welch MJ and Mach RH. Design and synthesis of 2-amino-4-methylpyridine analogues as inhibitors for inducible nitric oxide synthase and in vivo evaluation of [18F]6-(2-fluoropropyl)-4-methyl-pyridin-2-amine as a potential PET tracer for inducible nitric oxide synthase. J Med Chem 2009; 52: 2443-2453.

[142] Huang HJ, Isakow W, Byers DE, Engle JT, Griffin EA, Kemp D, Brody SL, Gropler RJ, Miller JP, Chu W, Zhou D, Pierce RA, Castro M, Mach RH and Chen DL. Imaging pulmonary inducible nitric oxide synthase expression with PET. J Nucl Med 2015; 56: 76-81.

[143] Herrero P, Laforest R, Shoghi K, Zhou D, Ewald G, Pfeifer J, Duncavage E, Krupp K, Mach R and Gropler R. Feasibility and dosimetry studies for 18F-NOS as a potential PET radiopharmaceutical for inducible nitric oxide synthase in humans. J Nucl Med 2012; 53: 994-1001.

[144] Yang X, Chordia MD, Du X, Graves JL, Zhang Y, Park YS, Guo Y, Pan D and Cui Q. Targeting formyl peptide receptor 1 of activated macrophages to monitor inflammation of experimental osteoarthritis in rat. J Orthop Res 2016; 34: 1529-1538.

[145] Helmy KY, Katschke KJ Jr, Gorgani NN, Kljavin NM, Elliott JM, Diehl L, Scales SJ, Ghilardi N and van Lookeren Campagne M. CRIg: a macrophage complement receptor required for phagocytosis of circulating pathogens. Cell 2006; 124: 915-927.

[146] Zheng F, Put S, Bouwens L, Lahoutte T, Matthys P, Muyldermans S, De Baetselier P, Devoogdt N, Raes G and Schoonooghe S. Molecular imaging with macrophage CRIg-targeting nanobodies for early and preclinical diagnosis in a mouse model of rheumatoid arthritis. J Nucl Med 2014; 55: 824-829.

[147] Muller A, Mu L, Meletta R, Beck K, Rancic Z, Drandarov K, Kaufmann PA, Ametamey SM, Schibli R, Borel N and Kramer SD. Towards non-invasive imaging of vulnerable atherosclerotic plaques by targeting co-stimulatory molecules. Int J Cardiol 2014; 174: 503-515.

[148] Meletta R, Steier L, Borel N, Mu L, Keller C, Chiotellis A, Russo E, Halin C, Ametamey SM, Schibli R, Kramer SD and Muller Herde A. CD80 is upregulated in a mouse model with shear stress-induced atherosclerosis and allows for evaluating CD80-targeting PET tracers. Mol Imaging Biol 2017; 19: 90-99.

[149] Eichendorff S, Svendsen P, Bender D, Keiding S, Christensen EI, Deleuran B and Moestrup SK. Biodistribution and PET imaging of a novel [68Ga]-anti-CD163-antibody conjugate in rats with collagen-induced arthritis and in controls. Mol Imaging Biol 2015; 17: 87-93.

[150] Hoffmann SHL, Reck DI, Maurer A, Fehrenbacher B, Sceneay JE, Poxleitner M, Oz HH, Ehrlichmann W, Reischl G, Fuchs K, Schaller M, Hartl D, Kneilling M, Moller A, Pichler BJ and Griessinger CM. Visualization and quantification of in vivo homing kinetics of myeloid-derived suppressor cells in primary and metastatic cancer. Theranostics 2019; 9: 5869-5885.

[151] Nigam S, McCarl L, Kumar R, Edinger RS, Kurland BF, Anderson CJ, Panigrahy A, Kohanbash G and Edwards WB. Preclinical immunoPET imaging of glioblastoma-infiltrating myeloid cells using zirconium-89 labeled anti-CD11b antibody. Mol Imaging Biol 2019; [Epub ahead of print].

[152] Cao Q, Huang Q, Mohan C and Li C. Small-animal PET/CT imaging of local and systemic immune response using (64)Cu-alphaCD11b. J Nucl Med 2019; 60: 1317-1324.

[153] Dmochowska N, Tieu W, Keller MD, Wardill HR, Mavrangelos C, Campaniello MA, Takhar P and Hughes PA. Immuno-PET of innate immune markers CD11b and IL-1beta detects inflammation in murine colitis. J Nucl Med 2019; 60: 858-863.

[154] Liu G, Hu Y, Xiao J, Li X, Li Y, Tan H, Zhao Y, Cheng D and Shi H. 99mTc-labelled anti-CD11b SPECT/CT imaging allows detection of plaque destabilization tightly linked to inflammation. Sci Rep 2016; 6: 20900.

[155] O'Neill AS, Terry SY, Brown K, Meader L, Wong AM, Cooper JD, Crocker PR, Wong W and Mullen GE. Non-invasive molecular imaging of inflammatory macrophages in allograft rejection. EJNMMI Res 2015; 5: 69.

[156] Terry SY, Boerman OC, Gerrits D, Franssen GM, Metselaar JM, Lehmann S, Oyen WJ, Gerdes CA and Abiraj K. ^{111}In-anti-F4/80-A3-1 anti-

body: a novel tracer to image macrophages. Eur J Nucl Med Mol Imaging 2015; 42: 1430-1438.

[157] Bigalke B, Phinikaridou A, Andia ME, Cooper MS, Schuster A, Wurster T, Onthank D, Munch G, Blower P, Gawaz M, Nagel E and Botnar RM. PET/CT and MR imaging biomarker of lipid-rich plaques using [64Cu]-labeled scavenger receptor (CD68-Fc). Int J Cardiol 2014; 177: 287-291.

[158] Rischpler C, Nekolla SG, Kossmann H, Dirschinger RJ, Schottelius M, Hyafil F, Wester HJ, Laugwitz KL and Schwaiger M. Upregulated myocardial CXCR4-expression after myocardial infarction assessed by simultaneous GA-68 pentixafor PET/MRI. J Nucl Cardiol 2016; 23: 131-133.